Life-Cycle Assessment of Long-Span Bridge's Wind Resistant Performance Considering Multisource Time-Variant Effects and Uncertainties

Article *in* Journal of Structural Engineering · July 2022

DOI: 10.1061/(ASCE)ST.1943-541X.0003388

CITATIONS
3

READS
139

4 authors:

Xiaolei Chu
University of California, Berkeley
6 PUBLICATIONS **17** CITATIONS
SEE PROFILE

Wei Cui
Tongji University
37 PUBLICATIONS **399** CITATIONS
SEE PROFILE

Lin Zhao
Tongji University
107 PUBLICATIONS **815** CITATIONS
SEE PROFILE

Yaojun Ge
Tongji University
162 PUBLICATIONS **1,541** CITATIONS
SEE PROFILE

Life-Cycle Assessment of Long-Span Bridge's Wind Resistant Performance Considering Multisource Time-Variant Effects and Uncertainties

Xiaolei Chu, S.M.ASCE[1]; Wei Cui, A.M.ASCE[2]; Lin Zhao[3]; and Yaojun Ge[4]

Abstract: This paper examines the life-cycle wind resistant performance of a constructed long-span suspension bridge in the coastal region of China, aiming to quantify the multisource time-variant effects and uncertainties and offering a reference for designs of long-span bridges in the future. Randomness from modal frequencies, damping ratios, and identification uncertainty of flutter derivatives (FDs) was considered; then, their effects on probability of flutter failure and probability of exceeding the predefined buffeting response root-mean square (RMS) are discussed. Firstly, results of full-track tropical cyclone (TC) simulation under various climate warming scenarios are reviewed; then, the time-variant probability density function (PDF) of annual extreme wind speed is discussed. Secondly, 6-year modal frequencies and damping ratios of a long-span suspension bridge with a center-slotted section were extracted by fast Bayesian FFT method with structural health monitoring (SHM) data, which were utilized to explore the deterioration rules of structural properties. Thirdly, FDs were modeled from a probabilistic perspective based on complex Wishart distribution, which were identified in the turbulent flow and the frequency domain by Bayesian inference. The posterior distributions of FDs, namely identification uncertainty, were quantified by Markov chain Monte Carlo (MCMC) sampling. This paper finds that for flutter resistant performance, the time-variant effects (i.e., modal frequencies and PDFs of extreme wind speed) will make the flutter failure probability seven times larger than the initial value; for the probability of exceeding the predefined buffeting response RMS, however, the time-variant effects will make a negligible difference. **DOI: 10.1061/(ASCE)ST.1943-541X.0003388.**

Author keywords: Long-span bridge; Typhoon hazard; Climate change; Structural deterioration; Flutter derivatives (FD); Uncertainty.

Introduction

Wind resistant of long-span bridges is paramount for structural safety. With the increasing occurrence of wind-related accidents, such as large-amplitude vortex-induced vibration (Li et al. 2011) and occupant comfort (Spence and Kareem 2014; Wang et al. 2022), wind resistant performance deserves more attention. In current engineering practice of wind-resistance design for long-span bridges, flutter instability (Caracoglia 2011), vortex-induced vibration (Zhang et al. 2021), and buffeting response root-mean square (RMS) (Seo and Caracoglia 2012) are three main issues for long-span bridges. Flutter resistant performance is related to two factors, onsite wind climate [i.e., probability density function (PDF) of annual extreme wind speed] and structural resistant capacity (i.e., flutter critical wind speed) (Seo and Caracoglia 2015), which threatens the structural safety and integrity. Large-amplitude vortex-induced vibration, tightly associated with damping ratios (Hwang et al. 2020), may cause inconvenience to traffic. Buffeting responses are an indicator for fatigue damage assessment (Xu et al. 2009; Gu et al. 1999), which are associated with modal frequencies, damping ratios, and flutter derivatives (Chen et al. 2000).

When it comes to in-service bridges, prediction and estimation of life-cycle wind resistant performance are much more important because onsite wind climate (Chen et al. 2021) and structural resistant capacity (Chu et al. 2021b; Yuen and Kuok 2010) are both time-variant, bringing significant uncertainty to structural safety. However, related investigations are still scarce. As a result, life-cycle assessment of wind resistant performance considering multisource time-variant effects and uncertainties is necessary, which will provide a comprehensive insight into long-term structural safety (Ellingwood and Lee 2016; Lee and Ellingwood 2017). This study focuses on effects of time-variant extreme wind speed in a warming climate (Chu et al. 2021a), structural health monitoring (SHM)-informed structural deterioration (Chu et al. 2021b), and uncertainties from modal properties and parametric inference (Chu et al. 2022); then, issues about life-cycle probability of flutter failure and probability of exceeding predefined buffeting response RMS are discussed.

Climate change is one of the severest challenges facing the Earth nowadays (Stocker 2014), where the warming effects are of much concern for structural designers because warming effects

[1]Graduate Student, State Key Lab of Disaster Reduction in Civil Engineering, Tongji Univ., Shanghai 200092, China. ORCID: https://orcid.org/0000-0001-5631-6571. Email: xiaoleichu@tongji.edu.cn

[2]Assistant Professor, State Key Lab of Disaster Reduction in Civil Engineering, Tongji Univ., Shanghai 200092, China; Assistant Professor, Key Laboratory of Transport Industry of Wind Resistant Technology for Bridge Structures, Tongji Univ., Shanghai 200092, China (corresponding author). ORCID: https://orcid.org/0000-0001-7489-923X. Email: cuiwei@tongji.edu.cn

[3]Professor, State Key Lab of Disaster Reduction in Civil Engineering, Tongji Univ., Shanghai 200092, China; Professor, Key Laboratory of Transport Industry of Wind Resistant Technology for Bridge Structures, Tongji Univ., Shanghai 200092, China; Professor, State Key Laboratory of Mountain Bridge and Tunnel Engineering, Chongqing Jiaotong Univ., Chongqing 400074, China. Email: zhaolin@tongji.edu.cn

[4]Professor, State Key Lab of Disaster Reduction in Civil Engineering, Tongji Univ., Shanghai 200092, China; Professor, Key Laboratory of Transport Industry of Wind Resistant Technology for Bridge Structures, Tongji Univ., Shanghai 200092, China. Email: yaojunge@tongji.edu.cn

Note. This manuscript was submitted on July 28, 2021; approved on March 2, 2022; published online on May 23, 2022. Discussion period open until October 23, 2022; separate discussions must be submitted for individual papers. This paper is part of the ***Journal of Structural Engineering***, © ASCE, ISSN 0733-9445.

can change typhoon activities and then affect the local wind environment (Xu et al. 2020). A large number of long-span bridges have been constructed along Chinese coastal regions, which often suffer from wind hazards (Zhao et al. 2019). For significant infrastructures, it is necessary to estimate the extreme wind speed through probabilistic methods from local wind speed records (Cui et al. 2021) or stochastic simulations (Hong et al. 2020; Hong and Li 2021). The first model is designated as the parent wind speed distribution, where hourly records extracted from a historical database of wind speeds from a meteorological station located in the adjacency of structures are utilized (Cui and Caracoglia 2015).

Another stochastic simulation model is to reproduce rare but intense tropical cyclones (TCs). Vickery et al. (2000a, b) firstly proposed the full-track TC simulation methodology on the basis of the historical TC tracks and intensities (Knapp et al. 2018). Inspired by Vickery et al. (2000a, b), many researchers developed their full-track TC model. Fang et al. (2021b) introduced the underlying terrain effects on TC wind speed in terms of a directional roughness length and a topographic speed-up factor, which helped to facilitate risk assessment and disaster mitigation during typhoon events. Fang et al. (2021a) also developed a forward-track model, based on geographically weighted regression, to incorporate the effects of the spatial heterogeneity on TC tracks and intensities. Wu et al. (2021a) adopted an enhanced circular subregion method for TC simulation, where Nataf transformation was introduced to incorporate the correlation among typhoon key parameters. Li and Hong (2021) employed the generalized density evolution equation to solve the probability distribution of the annual maximum typhoon surface wind speeds, where the typhoon motion was simulated by the beta-advection model, and the wind speed at a specific site was obtained by a three-dimensional nonlinear boundary layer wind field model. Shen and Wei (2021) incorporated the effects of ocean feedback on the TC intensities, improving the accuracy of TC simulation.

Recently, several researchers (Snaiki and Wu 2020; Cui and Caracoglia 2019) incorporated climate change effects on wind hazard analysis (Cui et al. 2020; Cui and Caracoglia 2016) and risk assessment (Pant and Cha 2019; Snaiki et al. 2020), where sea surface temperature (SST) was chosen to reflect potential effects of climate change. For example, Lee and Ellingwood (2017) adopted the Vickery model to infer the nonstationary intensities and frequencies of hurricanes under various climate warming scenarios for intergenerational decision model. Chen et al. (2021) developed a statistical dynamics synthetic TC model, which concluded that the warming climate would alter TC tracks, increase the proportion of supertyphoons, and then enhance the extreme wind speeds in most coastal areas of East Asia. In this study, estimation of annual extreme wind distributions in a warming climate [under different representative concentration pathways (RCPs), namely RCP2.6, RCP4.5, and RCP8.5 climate warming scenarios (Van Vuuren et al. 2011)] is reviewed, and then the time-variant wind environment is applied to the analysis of flutter failure probability.

It is normal practice to consider the reduction of modal frequencies as an indicator for structural deterioration (Salawu 1997). Based on structural response measurements, modal frequencies of the underlying structure can be identified, and any abnormal reduction is considered as an indicator of loss of structural integrity (Xia et al. 2006). However, some long-term monitoring studies revealed that the structural modal frequencies exhibited substantial seasonal variation without evidence of structural damage (Chu et al. 2021b). For example, Yuen and Kuok (2010) monitored a building and found that modal frequencies would be interfered with by the ambient conditions such as temperature and humidity, where modal frequencies and temperature showed a positive correlation. For long-span bridges, the seasonal variation is much more impactive because vortex-induced vibration is sensitive to damping ratios (Zhang et al. 2021). Also, the reduction of modal frequencies can lead to a decrease of flutter critical wind speed (Chu et al. 2021b), which is tightly related with flutter failure probability.

SHM data of civil infrastructure offer an opportunity to monitor and analyze long-term structural modal properties, which can be utilized to reveal the possible changing rules of bridges' modal properties under operational stage. Modal identification technologies of output-only systems have been deeply investigated. These technologies include the excitation technique (NExT) (James et al. 1993), random decrement technique (RDT) (Ibrahim 1977), frequency domain decomposition (FDD) (Brincker et al. 2001), wavelet (Peng et al. 2005), and stochastic subspace identification (SSI) (Hermans and Van der Auweraer 1999).

Another school (Beck 2010) viewed the modal identification as an inference about plausible system models, where Bayes' theorem was used to update the relative plausibility of each model in a model class. Probability logic with Bayesian updating, namely Bayesian system identification, has been a popular method recently (Yuen 2010). Both the most probable values (MPVs) and posterior distributions could be given, offering a rigorous framework for parametric inference (Beck 2010). Katafygiotis and Yuen (2001) proposed a Bayesian spectral density approach for modal updating, where the complex Wishart distribution was used to obtain not only the MPVs but also the posterior distributions. Yuen and Katafygiotis (2003) proposed a Bayesian fast Fourier transform (FFT) approach for modal updating and directly used the statistical characteristics of the Fourier transform of measured signals, avoiding the frequency-averaging process like many frequency-based approaches. The posterior distribution was quantified by the inverse Hessian matrix (Yuen and Katafygiotis 2003). Au (2011) proposed a fast Bayesian FFT algorithm for ambient model identification in the case of separated modes, and later he extended this algorithm to the general case of closely spaced modes (Au 2012a, b). Yuen and Katafygiotis (2001) also developed the Bayesian time-domain approach. Based on the fast Bayesian FFT method (Au 2011), in this study, structural deterioration effects of a long-span suspension bridge are discussed utilizing 6 years of continuous SHM data (Chu et al. 2021b). Hence, the time-variant flutter critical wind speed is discussed.

As for flutter derivatives (FDs), they can be utilized to estimate the flutter critical wind speed and buffeting responses (Scanlan and Tomo 1971). Due to intractable experimental conditions and different identification algorithms, the flutter derivatives are usually considered as random variables with large dispersion (Fang et al. 2020; Mannini and Bartoli 2015; Ji et al. 2020, 2021). Conventionally, there are two popular identification technologies to extract FDs in the wind-tunnel test. The first one is achieved by a forced vibration test (Zhao et al. 2020; Siedziako et al. 2017). The second one is by a free vibration test (Sarkar et al. 1992). Also, there are some stochastic algorithms developed utilizing buffeting responses, such as the SSI method (Gu and Qin 2004) and the unscented Kalman filter approach (Wu et al. 2021b). All these methods are operated in the time domain.

We all know long-term random vibration data can provide us with stable and reliable statistical properties, but to the authors' best knowledge, the identification framework for FDs is seldom developed in frequency domain using buffeting displacement responses. Furthermore, substantial emphasis is placed on experimental errors or experimental uncertainty (Seo and Caracoglia 2011), which means that the FDs are extracted at the same preset experimental conditions several times for statistical analysis (uncertainty is from model erection error or wind field error, among others). However, few researchers explained FDs from a probabilistic perspective, and

the uncertainty caused by conditions of measured signals has not been investigated sufficiently. Combined with buffeting displacement responses, the complex Wishart distribution (Krishnaiah 1976) offers us a tool to model the identification framework probabilistically. We can then discuss the FDs' identification uncertainty in the dynamic system using buffeting statistical properties (Chu et al. 2022), not just the experimental errors or experimental uncertainty.

Chu et al. (2022) named the uncertainty caused by conditions of measured signals as identification uncertainty, which is totally different from experimental errors or experimental uncertainty. Identification uncertainty actually describes the plausibility between the theoretical dynamic model [i.e., Scanlan's linear FD model (Scanlan and Tomo 1971) here] and the measured signals. Identification uncertainty comes from the accuracy of the predefined theoretical model, quality of measured signals, and so on. In fact, the posterior distribution is just the marginal distribution of a high-dimensional probability distribution (Chu et al. 2022). Certainly, people can also obtain and discuss the experimental errors or experimental uncertainty by the methodology used by Chu et al. (2022). They only need to repeat wind-tunnel experiments with the same preset conditions, similar with previous methods (Seo and Caracoglia 2011).

Inspired by Davenport's (1961) wind loading chain, we want to track the uncertainty alongside the chain and quantify the effects of multisource uncertainties on wind resistant capacities. In brief, this paper proposes a generalized framework for life-cycle assessment of flutter failure probability and exceeding probability of predefined buffeting response RMS. The whole assessment procedure is shown in Fig. 1. This study is expected to give an insight for life-cycle assessment of a long-span bridge's performance.

Annual Extreme Wind Speed Distribution in a Warming Climate

SST, the power source of TCs, has long been chosen as the representative factor for climate change when conducting typhoon or hurricane simulations using Vickery's empirical track model (Chu et al. 2021a; Lee and Ellingwood 2017; Cui and Caracoglia 2016). Different RCPs have been utilized to quantify different climate change effects (Stocker 2014), which are often used for projection of future SST. Usually, there are four climate warming scenarios: RCP2.6, RCP4.5, RCP6.0, and RCP8.5. According to the report from the International Panel on Climate Change (IPCC) (Stocker 2014), the magnitude stands for the possible range of radiative forcing values in the year 2100 relative to preindustrial values.

When employing Vickery's empirical track model, effects of climate change can be embodied by SST in the intensity equation (Vickery et al. 2000a). Combined with a TC's track, Georgiou's (1986) gradient wind field model is often used to obtain the wind speed of a specific place at the gradient height. The radius to maximum wind R_{max} and the Holland coefficient B are two significant parameters in Goergiou's model. Both parameters are data-driven and obtained based on regression analysis of historical observations. Fang et al. (2018) reformulated the explicit expressions of R_{max} and B in the northwestern Pacific Ocean. It should be stressed that the R_{max} and B used by Fang et al. (2018) are correct only if utilized in pair. Chu et al. (2021a) also incorporated the effects of SST on R_{max} by using a two-layer feed-forward neural network. For explanation, as shown in Fig. 2, we give the wind speed and direction joint PDFs of three representative cities along Chinese coastal regions by TC simulation, where the effects of climate change were not considered. Conservatively, we chose the extreme wind speed from all directions each year to calculate the PDF of annual typhoon extreme wind speed. It was found that a Gumbel distribution can fit the PDF well (Chu et al. 2021a).

Three RCP scenarios, RCP2.6, RCP4.5, and RCP8.5, are available from the open database (Flato et al. 2000), and we can conduct the full-track TC simulation under these three climate warming scenarios. In the context of climate change, the distribution parameters of annual extreme wind speed are no longer invariable. Chu et al. (2021a) discussed the time-variant distribution parameters of wind speed, as shown in Fig. 3, where estimated uncertainty was

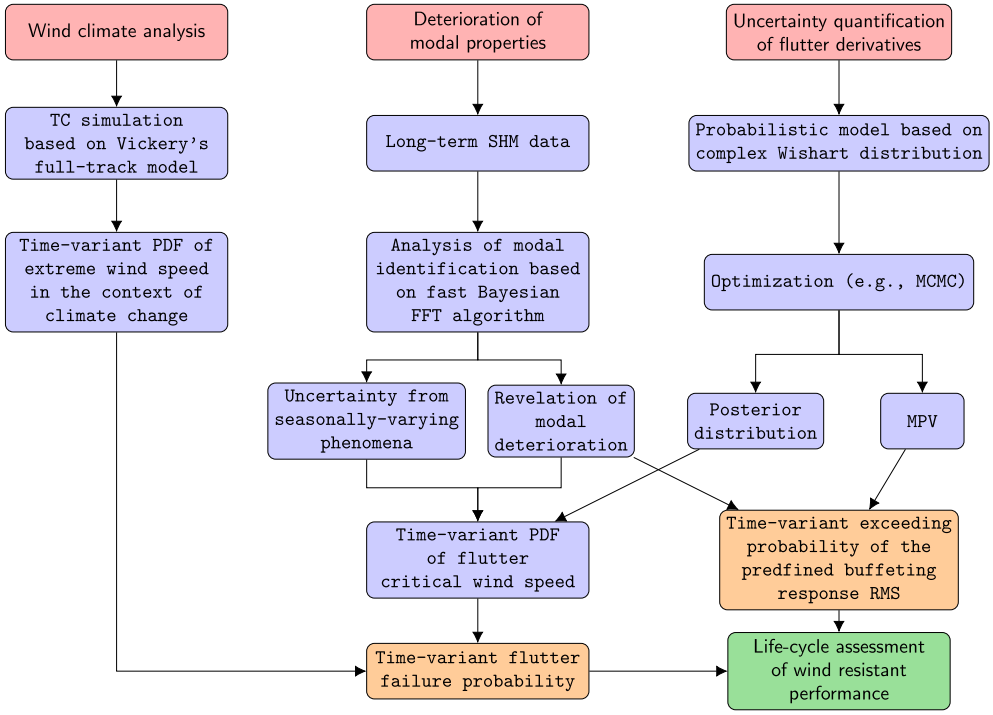

Fig. 1. Flowchart of life-cycle assessment for long-span bridge's wind resistant performance.

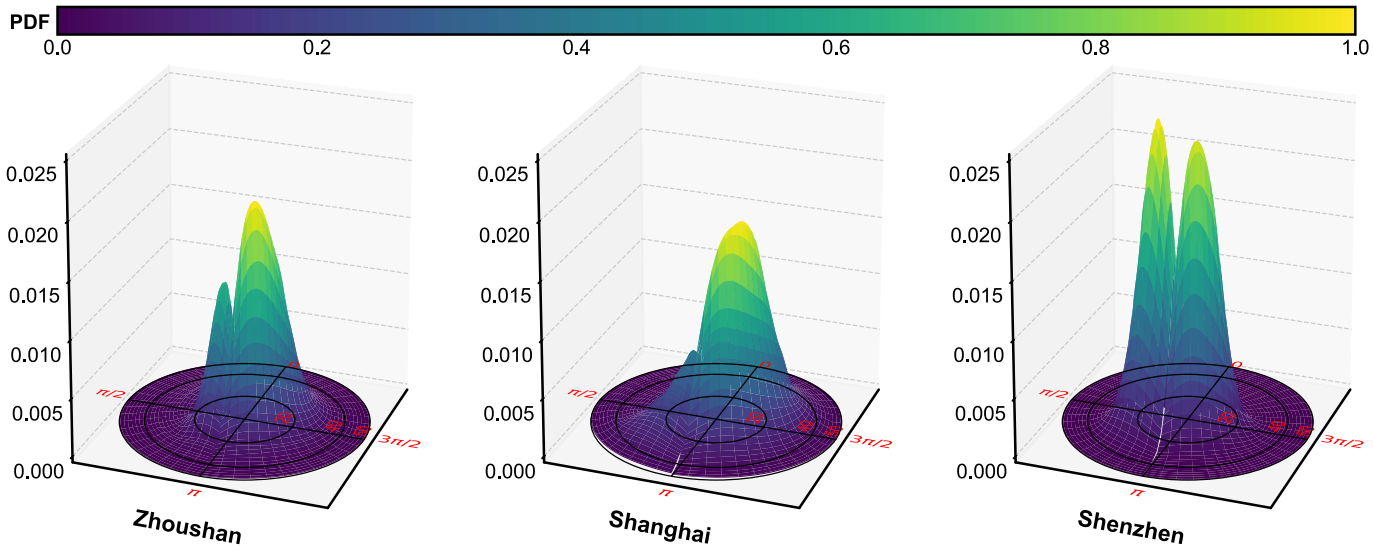

Fig. 2. Wind speed and direction joint PDF along Chinese coastal cities.

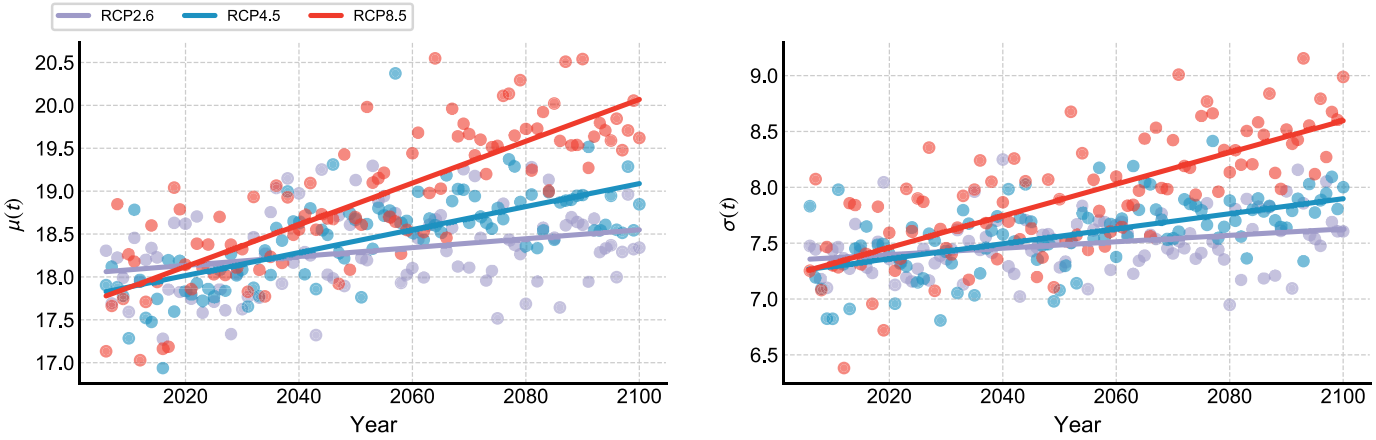

Fig. 3. Time-variant distribution parameters μ and σ of Gumbel distribution in Shenzhen, China.

quantified by the generalized density evolution equation (Li and Chen 2009). Effects of a warming climate on the PDF of the annual extreme wind speed were found to be location-dependent (Chu et al. 2021a); in some coastal regions of China (like Zhoushan), the effects are not remarkable. In order to manifest the effects of warming climate on the time-variant PDFs of annual extreme wind speed, Shenzhen, China, was taken as example, where PDFs were fitted by a Gumbel distribution (Chu et al. 2021a) as follows:

$$f(v|\mu_0(t),\sigma_0(t)) = \left(\frac{1}{\sigma_0(t)}\right)\exp\left(-\exp\left(-\frac{v-\mu_0(t)}{\sigma_0(t)}-\frac{v-\mu_0(t)}{\sigma_0(t)}\right)\right) \tag{1a}$$

$$\mu_0(t) = \begin{cases} 0.0052t + 7.6627(\text{RCP2.6}) \\ 0.0134t - 9.0499(\text{RCP4.5}) \\ 0.0244t - 31.0905(\text{RCP8.5}) \end{cases} \tag{1b}$$

$$\sigma_0(t) = \begin{cases} 0.0029t + 1.5787(\text{RCP2.6}) \\ 0.0067t - 6.2121(\text{RCP4.5}) \\ 0.0142t - 21.2088(\text{RCP8.5}) \end{cases} \tag{1c}$$

where $\mu_0(t)$ and $\sigma_0(t)$ = time-variant location parameter and scale parameter, respectively; and t = time, given as a future year (e.g., $t = 2{,}050$).

The magnitude of the scale in Fig. 4 indicates the PDF of the annual extreme wind speed. The red line is the fitted time-variant location parameter $\mu(t)$ in Fig. 3. Fig. 4 and the time-variant scale parameter in Fig. 3 also reveal that the variance of the wind speed varied intensely. Due to the long-tail effect, a small change in the wind speed PDF will alter the flutter probability significantly, as mentioned by Chu et al. (2021a).

Time-Variant Phenomena of Structural Properties

After construction, the modal properties (modal frequencies, damping ratios, and so on) of a structure are no longer the same as the initial values either due to structural deterioration (Chu et al. 2021b) or due to ambient interference (Yuen and Kuok 2010). Chu et al. (2021b) analyzed 6 years of SHM data of a long-span suspension bridge based on a fast Bayesian FFT identification algorithm. It was found that modal frequencies would decrease generally and fluctuate seasonally due to structural deterioration and seasonally

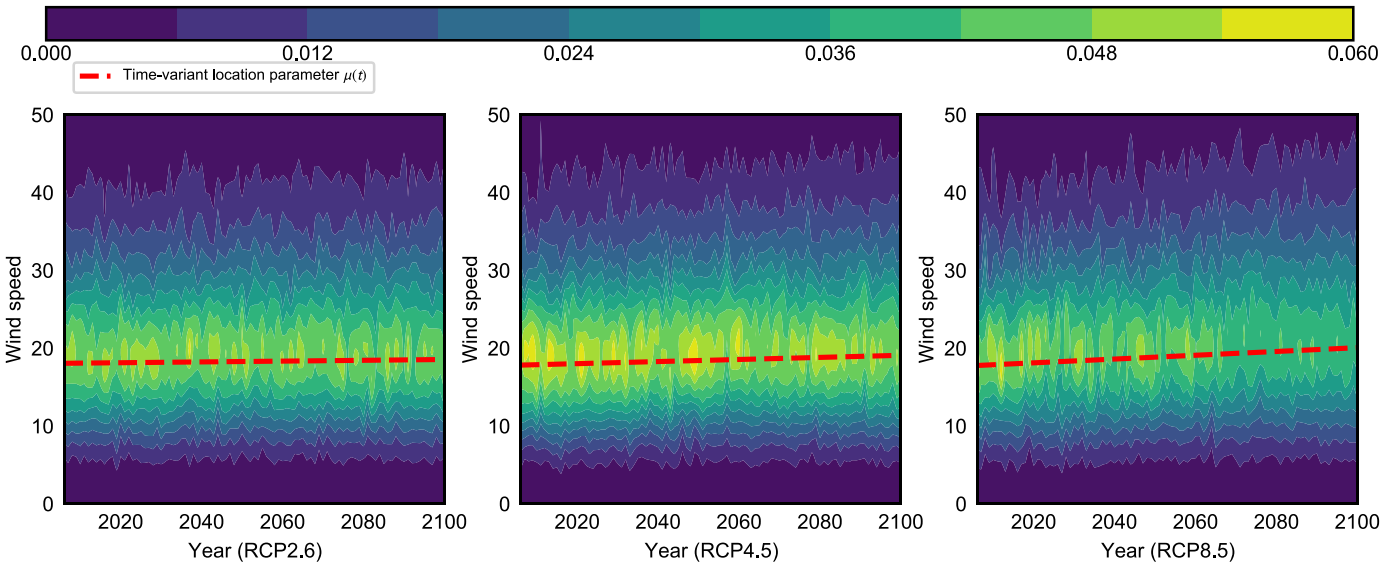

Fig. 4. Time-variant annual extreme wind speed distribution in Shenzhen, China.

varying ambient conditions, respectively, and damping ratios appeared to fluctuate seasonally only, which might also show deterioration effects if more SHM data are available (Chu et al. 2021b). In this section, the fast Bayesian FFT method (Au 2011) and the time-variant structural properties of that suspension bridge (Chu et al. 2021b) are discussed. More details have been given by Chu et al. (2021b).

Fast Bayesian FFT Method

Denote $\boldsymbol{\theta}$ as the set of modal parameters in which we are interested. Usually, $\boldsymbol{\theta}$ consists of modal frequency f_m, damping ratio ζ_m, mode shape ϕ_m, the power spectral density (PSD) of modal excitations S_m, and the PSD of the prediction error σ^2 (where m means the mth mode). Assuming a noninformative prior distribution, the posterior PDF $p(\boldsymbol{\theta}|\{\mathbf{Z}_k\})$ given the FFT data $\{\mathbf{Z}_k\}$ follows a Gaussian distribution with zero mean and covariance matrix $\mathbf{C}_k(\boldsymbol{\theta})$ (Katafygiotis and Yuen 2001), and $p(\boldsymbol{\theta}|\{\mathbf{Z}_k\})$ is proportional to the likelihood function $p(\{\mathbf{Z}_k\}|\boldsymbol{\theta})$ (where k is the frequency index)

$$p(\boldsymbol{\theta}|\{\mathbf{Z}_k\}) \propto p(\{\mathbf{Z}_k\}|\boldsymbol{\theta}) = (2\pi)^{-(N_q-1)/2}\left[\prod_{k=2}^{N_q}\det \mathbf{C}_k(\boldsymbol{\theta})\right]^{-1/2} \times \exp\left[-(1/2)\sum_{k=2}^{N_q}\mathbf{Z}_k^T\mathbf{C}_k(\boldsymbol{\theta})^{-1}\mathbf{Z}_k\right] \quad (2)$$

MPVs of modal properties $\hat{\boldsymbol{\theta}}$ can be determined by maximizing $p(\boldsymbol{\theta}|\{\mathbf{Z}_k\})$

$$\hat{\boldsymbol{\theta}} = \arg\max_{\boldsymbol{\theta}}\{p(\boldsymbol{\theta}|\{\mathbf{Z}_k\})\} \quad (3)$$

Actually, the fast Bayesian FFT method regards the identification problem as an optimization problem, where modal parameters $\boldsymbol{\theta}$ are inferred from the joint PDF. The identification algorithm is also frequency-domain but not time-domain, which means the identification accuracy does not heavily rely on the number of significant digits for each measurement.

Modal Frequencies

The time-variant deterioration functions of first-order vertical and torsional modal frequencies (Chu et al. 2021b), fitted in Fig. 5, are based on historical SHM data (from 2010 to 2015) of a suspension bridge. The results in Fig. 5 are monthly averaged due to missing data on certain days, so the variance does not seem obvious. Obviously, the modal frequencies are decreasing generally with bridge's aging due to various factors like material fatigues (Nguyen et al. 2019). The modal frequencies are also fluctuating seasonally, probably due to periodic temperature and humidity variation (Yuen and Kuok 2010).

The long-term deterioration functions are (Chu et al. 2021b)

$$f_h(t) = 0.09529\exp(-2.722\times10^{-5}\cdot 12t) + \epsilon_h \quad (4a)$$

$$f_\alpha(t) = 0.2372\exp(-2.596\times10^{-5}\cdot 12t) + \epsilon_\alpha \quad (4b)$$

where ϵ_h and ϵ_α = random variables fitted by residuals between measured frequencies and long-term deterioration functions in Fig. 5, PDFs of which are shown in Fig. 6. The unit of t is years, which means the time duration since construction.

Damping Ratios

Fig. 7 shows the 6-year variation of first-order vertical and torsional damping ratios. The long-term deterioration phenomenon of damping ratios is ambiguous, however, the seasonally varying characteristic is much more remarkable. There existed large damping ratios on certain summer days, which may be caused by anomalous high temperatures or relatively large deflection amplitudes of the bridge deck (Yuen and Kuok 2010). With a longer time duration, the long-term deterioration may also appear (Chu et al. 2021b).

As a result, in this study, we regard damping ratios as time-invariant random variables, the PDFs of which are fitted by 6-year measured data (i.e., Fig. 7) directly, as shown in Fig. 8.

Bayesian Spectral Density Approach for Identification and Uncertainty Quantification of Flutter Derivatives

In order to discuss the identification uncertainty of the bridge section model, we briefly introduce the complex Wishart distribution

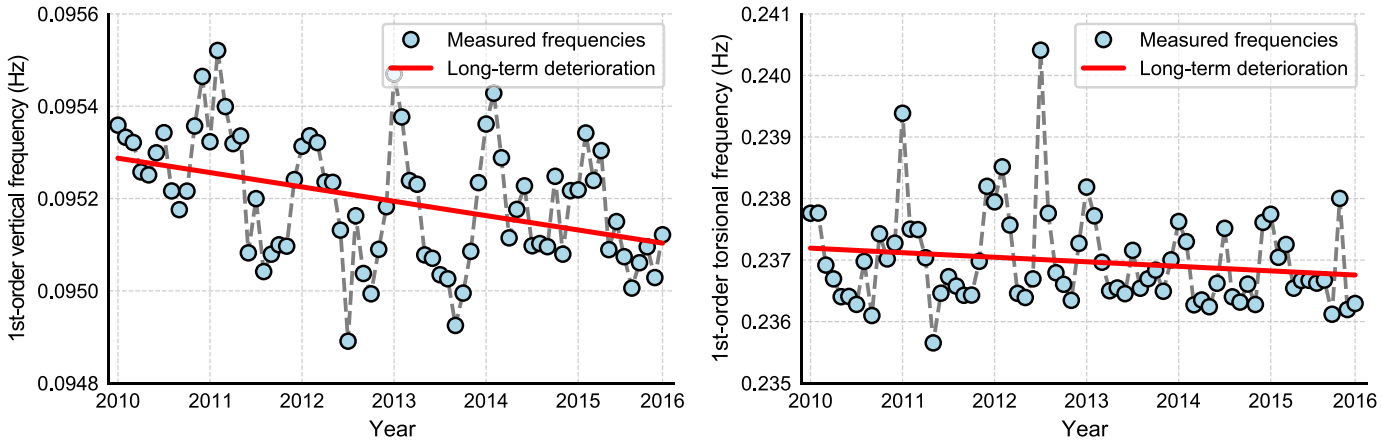

Fig. 5. Long-term deteriorations and corresponding seasonally varying characteristics of modal frequencies.

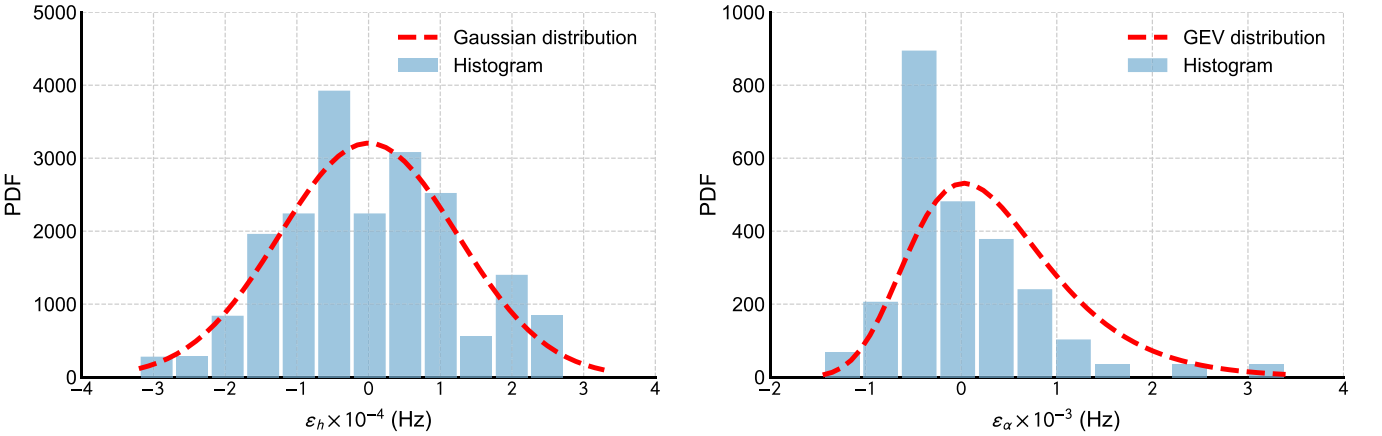

Fig. 6. First-order vertical and torsional modes: PDFs of seasonal fluctuations of modal frequencies, fitted by regression residuals.

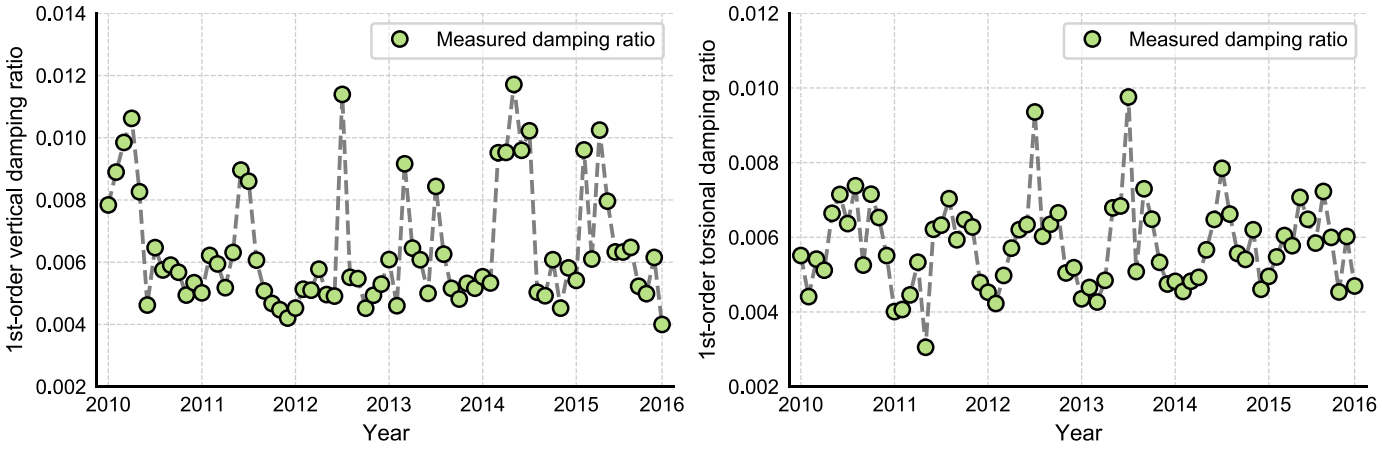

Fig. 7. Seasonally varying characteristics of damping ratios.

here, which offers a rigorous framework for parametric inference in a stochastic process (Krishnaiah 1976). Yuen (2010) successfully applied it (namely the Bayesian spectral density approach) to structural health monitoring to identify modal frequencies, damping ratios, and mode shapes of a constructed structure. In this section, this framework is applied to infer FDs (operated in turbulent flow) in the frequency domain. Detailed mathematical derivations have been given by Chu et al. (2022).

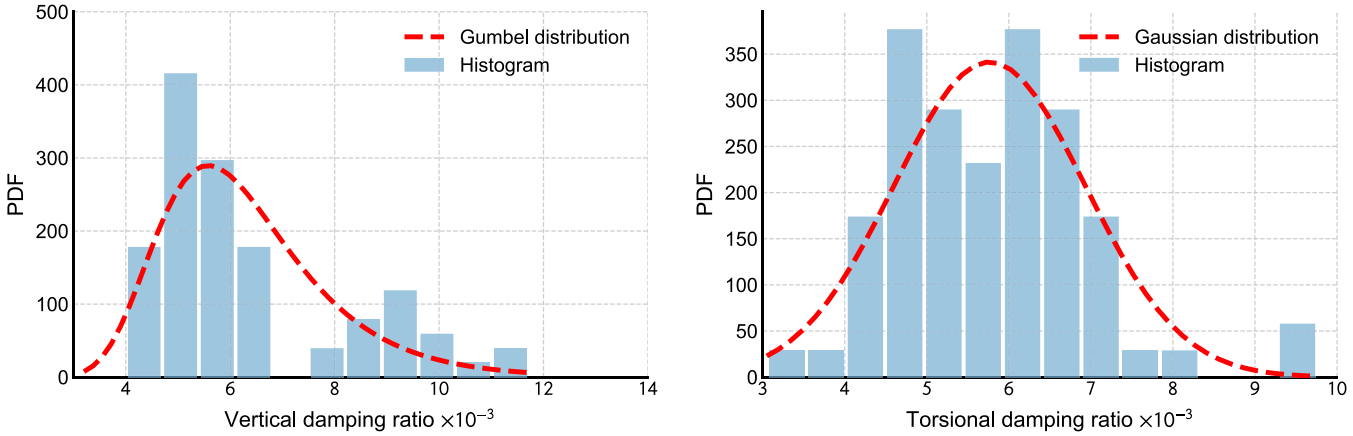

Fig. 8. First-order vertical and torsional modes: PDFs of damping ratios.

Theoretical Bridge Section Model in Frequency Domain

In the wind-tunnel test, a bridge section model with two degrees of freedom (DOFs), i.e., h (vertical motion) and α (torsional motion), is often utilized. The dynamic behavior of the section model in turbulent flow can be described by the following equations:

$$\boldsymbol{M}\ddot{\boldsymbol{x}}(t)+\boldsymbol{C}\dot{\boldsymbol{x}}(t)+\boldsymbol{K}\boldsymbol{x}(t)=\boldsymbol{f}(t) \tag{5a}$$

$$\boldsymbol{M}=\begin{bmatrix}1 & 0\\ 0 & 1\end{bmatrix},\quad \boldsymbol{C}=\begin{bmatrix}2\zeta_h\omega_h-H_1 & -H_2\\ -A_1 & 2\zeta_\alpha\omega_\alpha-A_2\end{bmatrix},\quad \boldsymbol{K}=\begin{bmatrix}\omega_h^2-H_4 & -H_3\\ -A_4 & \omega_\alpha^2-A_3\end{bmatrix} \tag{5b}$$

$$H_1=\frac{\rho B^2\omega_h}{m}H_1^*(K_h),\quad H_2=\frac{\rho B^3\omega_\alpha}{m}H_2^*(K_\alpha),$$
$$H_3=\frac{\rho B^3\omega_\alpha^2}{m}H_3^*(K_\alpha),\quad H_4=\frac{\rho B^2\omega_h^2}{m}H_4^*(K_h),$$
$$A_1=\frac{\rho B^3\omega_h}{I}A_1^*(K_h),\quad A_2=\frac{\rho B^4\omega_\alpha}{I}A_2^*(K_\alpha),$$
$$A_3=\frac{\rho B^4\omega_\alpha^2}{I}A_3^*(K_\alpha),\quad A_4=\frac{\rho B^3\omega_h^2}{I}A_4^*(K_h) \tag{5c}$$

where H_i^* and $A_i^*(i=1,2,3,4)$ = FDs ; m and I = mass and the mass moment of inertia of the deck per unit span, respectively; ω_i = natural circular frequency; ζ_i = damping ratio $(i=h,\alpha)$; ρ = air mass density; B = width of the bridge deck; U = mean wind speed at the bridge deck level; $K_i=\omega_i B/U$ is the reduced frequency $(i=h,\alpha)$; $\boldsymbol{x}(t)=[h(t),\alpha(t)]^T$ is the buffeting displacement response vector; and $\boldsymbol{f}(t)=[(1/m)L_b(t),(1/I)M_b(t)]^T$, where $L_b(t)$ and $M_b(t)$ are buffeting forces. It should be stressed that due to the selection of linear Scanlan's FDs, nonlinear effects were not considered. This issue needs to be clarified in future research.

The frequency response function of the 2-DOF model is

$$\mathbf{H}(\omega)=(\boldsymbol{K}-\omega^2\boldsymbol{M}+\mathrm{i}\omega\boldsymbol{C})^{-1} \tag{6}$$

where $\mathbf{H}(\omega)$ = frequency response function; and ω = circular frequency.

In the classical buffeting theory, the buffeting forces were expressed by means of aerodynamic admittance functions (Chen et al. 2000; Diana et al. 2020a, b), which were dependent on frequency and bridge deck profiles. However, in this study, information about aerodynamic admittance functions was not necessary because we only needed the information about buffeting forces' PSDs in a selected narrow band. It is reasonable to simplify the buffeting force as a narrow-band Gaussian white noise in that selected frequency band. Also buffeting forces' PSDs are just parameters to be inferred. A similar simplification was used by Wu et al. (2021b). As a result, we neglected the cross-spectrum of buffeting forces; then, the PSD matrix of buffeting displacement response $\boldsymbol{x}$ is

$$\begin{aligned}\mathbf{S}_x(\omega)&=\begin{bmatrix}S_{hh}(\omega) & S_{h\alpha}(\omega)\\ S_{\alpha h}(\omega) & S_{\alpha\alpha}(\omega)\end{bmatrix}\\&=\mathbf{H}(\omega)\mathbf{S}_f(\omega)\mathbf{H}^*(\omega)\\&=\mathbf{H}(\omega)\begin{bmatrix}S_L(\omega) & 0\\ 0 & S_M(\omega)\end{bmatrix}\mathbf{H}^*(\omega)\end{aligned} \tag{7}$$

where $(\cdot)^*$ = conjugate transpose of $(\cdot)$. Within the adjacent and narrow band around resonant circular frequencies $\mathcal{K}^{(h)}$ (around ω_h) and $\mathcal{K}^{(\alpha)}$ (around ω_α), $S_L(\omega)$ and $S_M(\omega)$ can be considered as constants in the respective frequency ranges, denoted as $(S_{L,h}, S_{L,\alpha})$ and $(S_{M,h}, S_{M,\alpha})$ (Chu et al. 2022).

Application of the Complex Wishart Distribution

Denote all parameters to be inferred as $\boldsymbol{\theta}=\{A_i,H_i,S_{L,h},S_{L,\alpha},S_{M,h},S_{M,\alpha}\}(i=1,2,3,4)$. We can infer $\boldsymbol{\theta}$ in the frequency domain based on the complex Wishart distribution (Krishnaiah 1976) as follows:

$$p[\mathbf{S}_N^M(\omega_k)|\boldsymbol{\theta}]=\frac{\pi^{-1}M^{M+2}|\mathbf{S}_N^M(\omega_k)|^{M-2}}{[\prod_{p=1}^2(M-p)!]|\mathbb{E}[\mathbf{S}_N(\omega_k)|\boldsymbol{\theta}]|^M}\times\exp(-M\cdot\mathrm{tr}\{\mathbb{E}[\mathbf{S}_N(\omega_k)|\boldsymbol{\theta}]^{-1}\mathbf{S}_N^M(\omega_k)\}) \tag{8}$$

where M = number of independent signals for inference; $\mathbf{S}_N^M$ = average of measured independent signals; $\mathrm{tr}\{\cdot\}$ = trace of a matrix; and $\mathbb{E}[\mathbf{S}_N(\omega_k)|\boldsymbol{\theta}]$ is obtained by Eq. (7).

In the Bayesian context, the posterior distribution can be established

$$p(\boldsymbol{\theta}|\mathbf{S}_N^{M,\mathcal{K}^{(h)},\mathcal{K}^{(\alpha)}})=\kappa p(\boldsymbol{\theta})\prod_{k\in\mathcal{K}^{(h)}}p[\mathbf{S}_N^M(k)|\boldsymbol{\theta}]\cdot\prod_{k\in\mathcal{K}^{(\alpha)}}p[\mathbf{S}_N^M(k)|\boldsymbol{\theta}] \tag{9}$$

where κ =normalizing constant; $p(\boldsymbol{\theta}|\mathbf{S}_N^{M,\mathcal{K}^{(h)},\mathcal{K}^{(\alpha)}})$ = posterior distribution; and $p(\boldsymbol{\theta})$ = prior distribution.

The posterior distribution of $\boldsymbol{\theta}$ (i.e., the identification uncertainty) can be obtained. The MPV $\hat{\boldsymbol{\theta}}$ is

$$\hat{\boldsymbol{\theta}} = \arg\max_{\boldsymbol{\theta}}[p(\boldsymbol{\theta}|\mathbf{S}_N^{M,\mathcal{K}^{(h)},\mathcal{K}^{(\alpha)}})] \tag{10}$$

It should be stressed that the prior distribution $p(\boldsymbol{\theta})$ is very important for Bayesian inference because it can affect the posterior distribution $p(\boldsymbol{\theta}|\mathbf{S}_N^{M,\mathcal{K}^{(h)},\mathcal{K}^{(\alpha)}})$ significantly. If we have no prior knowledge (which is often the case), we usually consider $p(\boldsymbol{\theta})$ as a uniform distribution in a limited interval. Or in the application of structural modal identification, $p(\boldsymbol{\theta})$ is often neglected. In that case, Bayesian inference is no different from maximum likelihood estimation (Au 2017). In our case, we suggest people not neglect $p(\boldsymbol{\theta})$ because we have 12 parameters to be inferred, much more than those in the case of modal identification [only four were used by Au (2011)]. Also, neglecting $p(\boldsymbol{\theta})$ often leads to nonconvergence, especially when using MCMC. We suggest people start the optimization with an initial guess around the Theodorsen solutions (Scanlan 1993), and the interval of the prior distributions could be selected around the Theodorsen solutions.

The validity of this proposed identification algorithm has been investigated by Chu et al. (2022) by comparing the identified results of a thin plate with the Theodorsen results. In this subsection, we give the identified results of a center-slotted bridge [the cross-section model used by Chu et al. (2022)] when the mean wind speed in the wind tunnel is $U = 7.25$ m/s ($K_h = 1.4547$ and $K_\alpha = 2.3399$), as shown in Figs. 9 and 10, for the sake of explanation.

Fig. 10 shows the marginal distributions of FDs when the mean wind speed is 7.25 m/s. The marginal distributions were approximately normally distributed, where the one standard deviation σ bound is also given. When calculating the PDF of the flutter critical wind speed, the samples of FDs were chosen from the one standard deviation σ bound. As we have mentioned, due to different selections of prior distribution models, the posterior distribution (i.e., identification uncertainty) will be different. We find that if the prior distributions were chosen as uniform distribution around the Theodorsen solutions, $\sigma/|\text{MPV}|$ was about 10%–50% dependent on the interval length of the uniform distribution. In this study, we chose $\sigma/|\text{MPV}| = 20\%$ as the identification uncertainty.

Fig. 11 shows the measured buffeting response PSDs and the reconstructed buffeting response PSDs with identified MPVs (i.e., FDs and buffeting force PSDs). The reconstructed PSDs were consistent with the measured ones, which means that the identified results are correct. We proposed a nondimensional indicator λ to examine the consistency, as shown in Eq. (11). The closer the indicator is to 1, the more accurate the identified result

$$\lambda = \frac{(n\sum_k\{\mathbb{E}[\mathrm{S}_{i,N}(\omega_k)|\hat{\boldsymbol{\theta}}]\mathrm{S}_{i,N}^M(\omega_k)\} - \sum_k \mathbb{E}[\mathrm{S}_{i,N}(\omega_k)|\hat{\boldsymbol{\theta}}] \cdot \sum_k \mathrm{S}_{i,N}^M(\omega_k))^2}{\left(n\sum_k(\mathbb{E}[\mathrm{S}_{i,N}(\omega_k)|\hat{\boldsymbol{\theta}}])^2 - (\sum_k \mathbb{E}[\mathrm{S}_{i,N}(\omega_k)|\hat{\boldsymbol{\theta}}])^2)(n\sum_k(\mathrm{S}_{i,N}^M(\omega_k))^2 - (\sum_k \mathrm{S}_{i,N}^M(\omega_k))^2\right)} \tag{11}$$

where $k \in \{\mathcal{K}^{(h)}, \mathcal{K}^{(\alpha)}\}$; n = number of elements in $\{\mathcal{K}^{(h)}, \mathcal{K}^{(\alpha)}\}$; $\mathbb{E}[\mathrm{S}_{i,N}(\omega_k)|\hat{\boldsymbol{\theta}}]$ = reconstructed PSD with identified MPVs $\hat{\boldsymbol{\theta}}$ at frequency ω_k; and $\mathrm{S}_{i,N}^M(\omega_k)$ = measured PSD at frequency ω_k; $i = (hh, \alpha\alpha)$, as denoted in Eq. (7).

The FDs at various reduced velocities can be obtained by changing the mean wind speed U (Chu et al. 2022).

Life-Cycle Assessment Methodology for Wind Resistant Performance of Long-Span Bridges

Evaluation of Flutter Failure Probability

When it comes to flutter failure probability, factors can be categorized into two aspects, structural flutter resistance ability V_R (i.e., flutter critical wind speed) and wind load effect V_S (i.e., extreme wind speed). In flutter analysis, V_R is the function of modal frequencies $\boldsymbol{f}(t;\boldsymbol{\Theta}_f)$, damping ratios $\boldsymbol{\zeta}(t;\boldsymbol{\Theta}_\zeta)$, and flutter derivatives $\mathbf{A}^*$ (A_1^*, A_2^*, A_3^*, A_4^*; $\boldsymbol{\Theta}_\mathbf{A}$) and $\mathbf{H}^*$ (H_1^*, H_2^*, H_3^*, H_4^*; $\boldsymbol{\Theta}_\mathbf{H}$). Denote $\boldsymbol{\Theta} = \boldsymbol{\Theta}(\boldsymbol{\Theta}_f, \boldsymbol{\Theta}_\zeta, \boldsymbol{\Theta}_\mathbf{A}, \boldsymbol{\Theta}_\mathbf{H})$, which is the time-invariant uncertainty embedded in flutter critical wind speed. Structural properties $(\boldsymbol{f}(t), \boldsymbol{\zeta}(t))$ will be time-variant due to aging and environmental factors based on SHM data (Chu et al. 2021b). V_S is the time-variant extreme wind speed, which can be obtained by TC simulations (Chu et al. 2021a). Based on V_R and V_S, a state function Z can be defined

$$\begin{aligned} Z(V_R(t), V_S(t);\boldsymbol{\Theta}) &= V_R(\boldsymbol{f}(t;\boldsymbol{\Theta}_f), \boldsymbol{\zeta}(t;\boldsymbol{\Theta}_\zeta), \mathbf{A}^*(\boldsymbol{\Theta}_\mathbf{A}), \mathbf{H}^*(\boldsymbol{\Theta}_\mathbf{H})) \\ &\quad - V_S(t;\mu_0(t),\sigma_0(t)) \\ &= V_R(t;\boldsymbol{\Theta}) - V_S(t;\mu_0(t),\sigma_0(t)) \end{aligned} \tag{12}$$

where $Z < 0$ means the occurrence of flutter; $\mathbb{E}[Z < 0]$ = flutter failure probability; $\boldsymbol{\Theta}_f$ is shown in Fig. 6; $\boldsymbol{\Theta}_\zeta$ is shown in Fig. 8; $\boldsymbol{\Theta}_\mathbf{A}$ and $\boldsymbol{\Theta}_\mathbf{H}$ are shown in Fig. 10; $\mu_0(t)$ and $\sigma_0(t)$ are obtained from Eq. (1*a*); and t = structural age.

The time-variant PDFs of V_R and V_S are denoted as $p_R(r,t)$ and $p_S(s,t)$, respectively. Thus, the time-variant flutter failure probability (Melchers and Beck 2018) is

$$\begin{aligned} P_f(t) &= P(Z<0) \\ &= P(V_R(t;\boldsymbol{\Theta}) - V_S(t;\mu_0(t),\sigma_0(t)) < 0) \\ &= \int\int_{r<s} p_{RS}(r,s,t)\mathrm{d}r\mathrm{d}s \\ &= \int\int_{r<s} p_R(r,t)\cdot p_S(s,t)\mathrm{d}r\mathrm{d}s \\ &= \int_{-\infty}^{+\infty}\left[\int_{-\infty}^{s} p_R(r,t)\mathrm{d}r\right]\cdot p_S(s,t)\mathrm{d}s \end{aligned} \tag{13}$$

Evaluation of Exceeding Probability of Predefined Buffeting Response RMS

In this subsection, the emphasis is placed on the buffeting response RMS. Buffeting response is related to turbulent intensity, turbulent length scale, and so on (Liu et al. 2021). The effects of climate change on the local wind environment (e.g., turbulent intensity and turbulent length) have not been investigated thoroughly, so the effects of climate change were not considered in the discussion of buffeting response RMS [i.e., S_L and S_M in Eq. (7) are time-invariant]. FDs are only related with the bridge profile and reduced velocities, which are also time-invariant. In order to reveal the

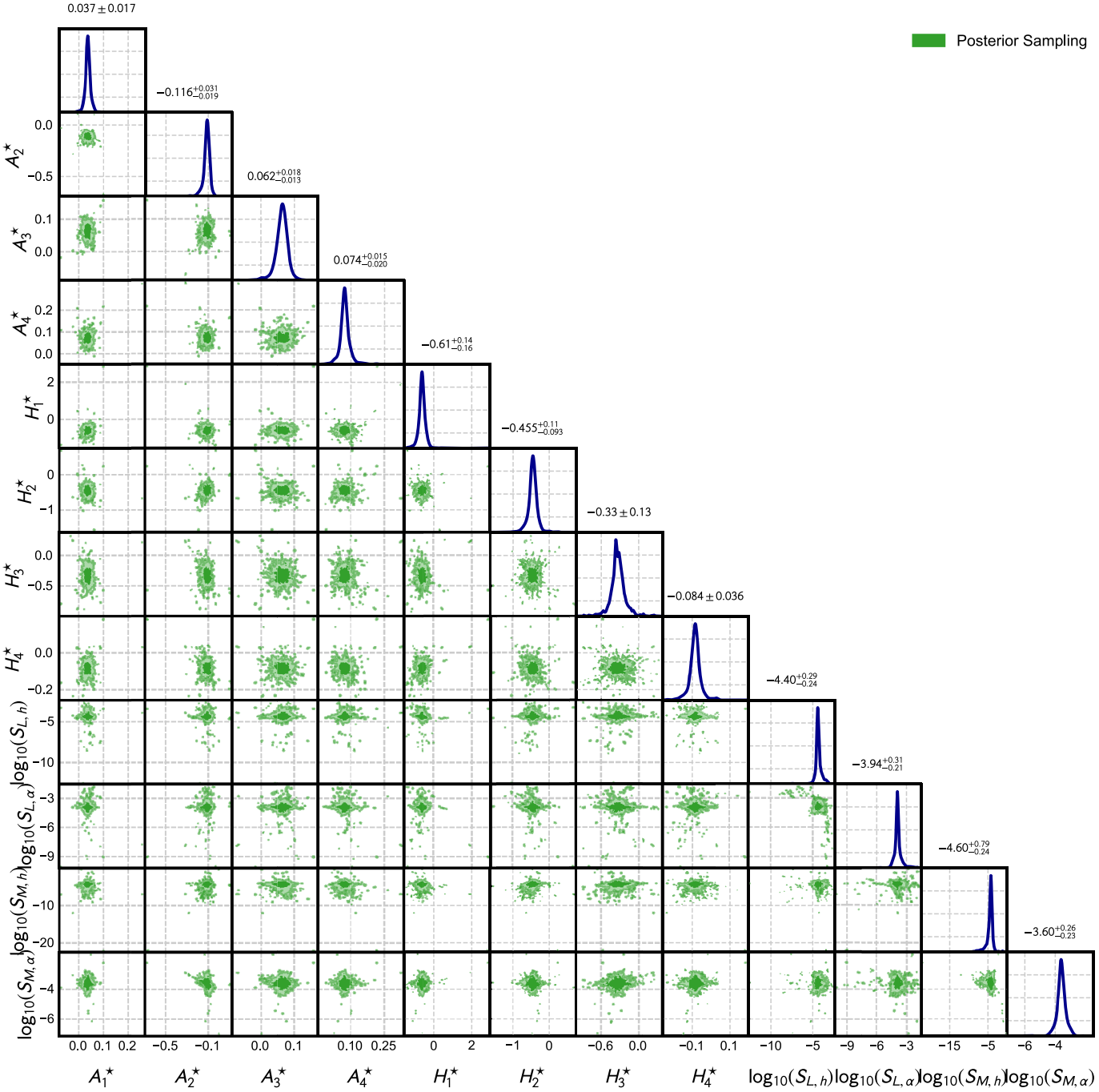

Fig. 9. Posterior distribution of FDs when $U = 7.25$ m/s ($K_h = 1.4547$ and $K_\alpha = 2.3399$).

potential effects of structural deterioration on buffeting response RMS, the same reduction rate of modal frequencies in Eq. (4) was employed here. The uncertainty $\boldsymbol{\Theta}$ was not considered in the buffeting analysis.

We utilized the identified time-invariant MPVs of $\boldsymbol{\theta} = \{A_i, H_i, S_{L,h}, S_{L,\alpha}, S_{M,h}, S_{M,\alpha}\}(i = 1, 2, 3, 4)$ and experimental modal frequencies with the same deteriorating rate in Eq. (4) to reconstruct the buffeting response PSDs; then, the buffeting response RMS was the square root of the buffeting response PSDs' integrals over the whole frequency domain. As mentioned by Gu et al. (1999), when estimating the integrals of PSDs, the integrating ranges can be chosen to be around the modal frequencies f_h and f_α (i.e., $\mathcal{K}^{(h)}$ and $\mathcal{K}^{\alpha}$). The other background PSDs are negligible (Gu et al. 1999). The vertical buffeting response was nondimensionalized by dividing the depth of the bridge. Fig. 12 shows the comparison between measured RMS and estimated RMS (with identified MPVs of FDs and buffeting force PSDs over $\mathcal{K}^{(h)}$ and $\mathcal{K}^{(\alpha)}$), which means that the estimation is reasonable.

Then, the life-cycle buffeting response RMS can be estimated as follows:

$$\sigma_{hh}(t) \approx \sqrt{\int_{\omega \in 2\pi\mathcal{K}^{(h)}} S_{hh}(\omega, t)\mathrm{d}\omega + \int_{\omega \in 2\pi\mathcal{K}^{(\alpha)}} S_{hh}(\omega, t)\mathrm{d}\omega} \quad (14a)$$

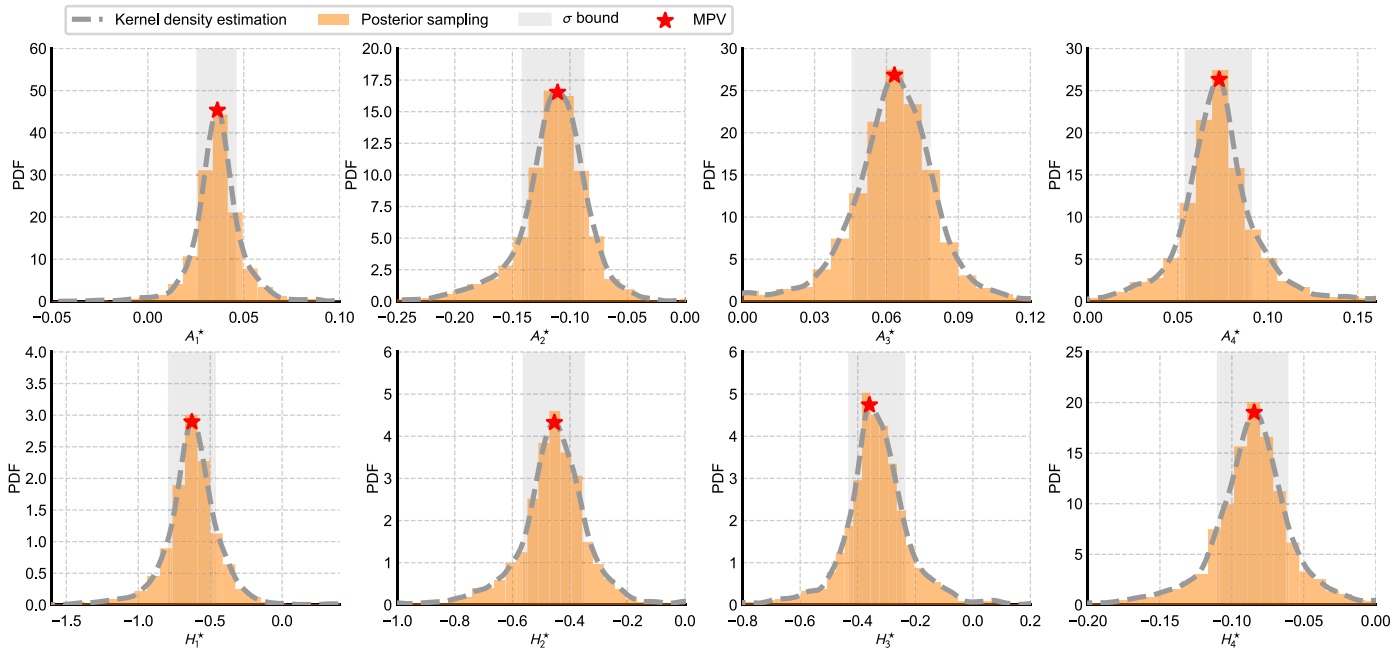

Fig. 10. Marginal distribution of FDs when $U = 7.25$ m/s ($K_h = 1.4547$ and $K_\alpha = 2.3399$).

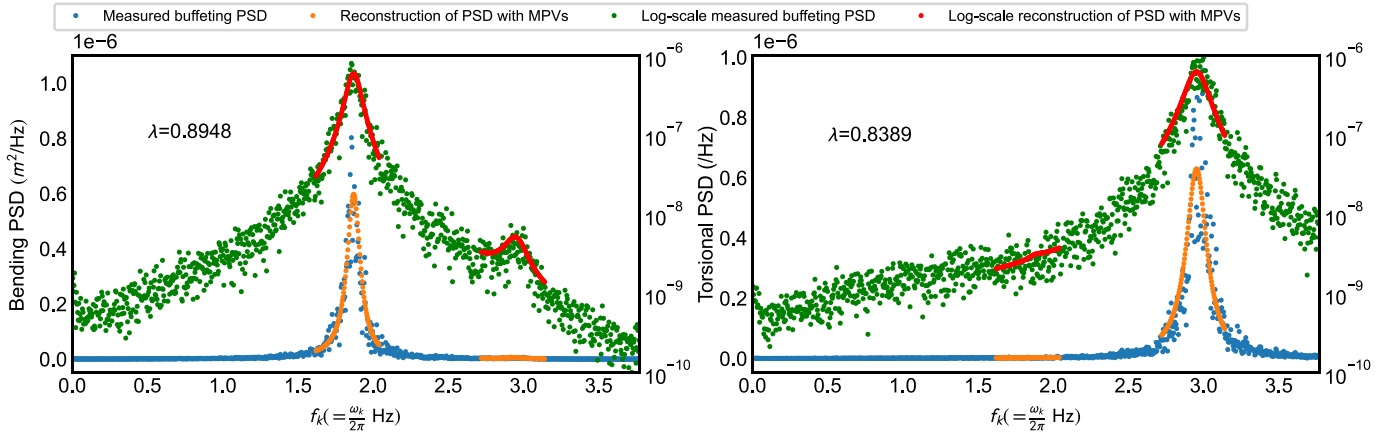

Fig. 11. Measured buffeting response PSDs and reconstruction of buffeting response PSDs with identified MPVs, i.e., FDs and buffeting force PSDs, when $U = 7.25$ m/s ($K_h = 1.4547$ and $K_\alpha = 2.3399$).

$$\sigma_{\alpha\alpha}(t) \approx \sqrt{\int_{\omega\in 2\pi\mathcal{K}^{(h)}} S_{\alpha\alpha}(\omega,t)\mathrm{d}\omega + \int_{\omega\in 2\pi\mathcal{K}^{(\alpha)}} S_{\alpha\alpha}(\omega,t)\mathrm{d}\omega} \quad (14b)$$

where t = structural age; and S_{hh} and $S_{\alpha\alpha}$ can be obtained by Eq. (7) and are time-variant due to the deteriorating modal frequencies.

Assuming the predefined limit of buffeting response RMS is σ_{lim}, the exceeding probability is

$$P(\sigma(t) > \sigma_{\text{lim}}) = P(v(t) > v_{\text{lim}}(t);\ \mu_0(t), \sigma_0(t)) \quad (15)$$

where $v(t)$ and $v_{\text{lim}}(t)$ = wind speeds corresponding to the buffeting response RMS $\sigma(t)$ and σ_{lim}; and $\mu_0(t)$ and $\sigma_0(t)$ = time-variant Gumbel distribution parameters in Eq. (1*a*).

Application of Proposed Life-Cycle Assessment Methodology

Time-Variant Flutter Failure Probability

With the modal frequencies' deteriorating, as shown in Fig. 13, the flutter critical wind speed will decay. The scale used in Fig. 13 indicates the PDF of flutter critical wind speed. The randomness of the flutter critical wind speed comes from residuals between measured frequencies and long-term deterioration functions (Fig. 6), seasonally varying damping ratios (Fig. 8), and identification uncertainty of FDs (Fig. 10). Fig. 13 shows that the fitted expectation of flutter critical wind speed (denoted as the green line) will approximately decrease from 91.2 to 88.9 m/s. In Fig. 13, the uncertainty

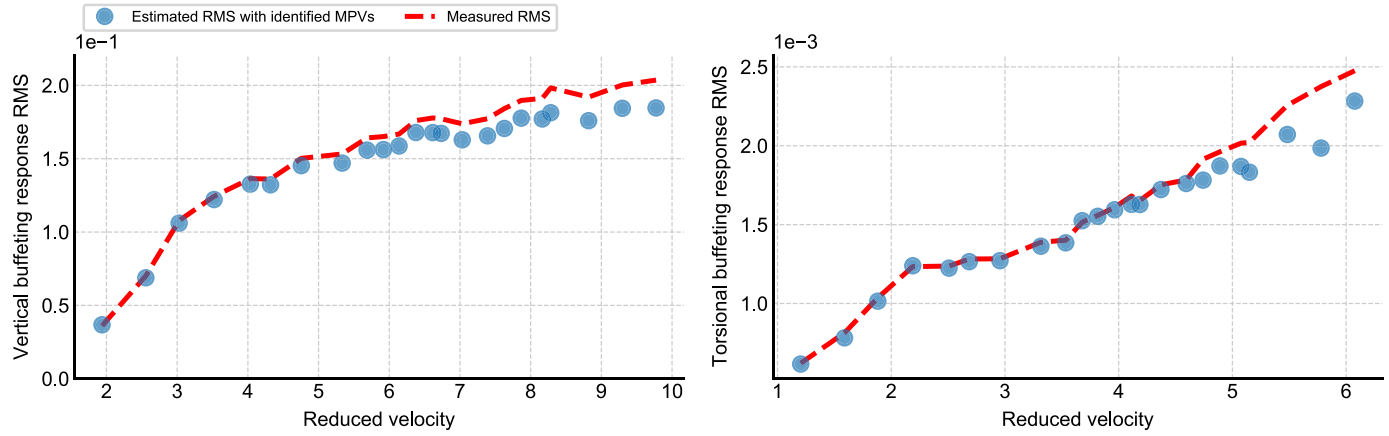

Fig. 12. Measured buffeting response RMS and estimated buffeting response RMS with identified MPVs (i.e., FDs and buffeting force PSDs).

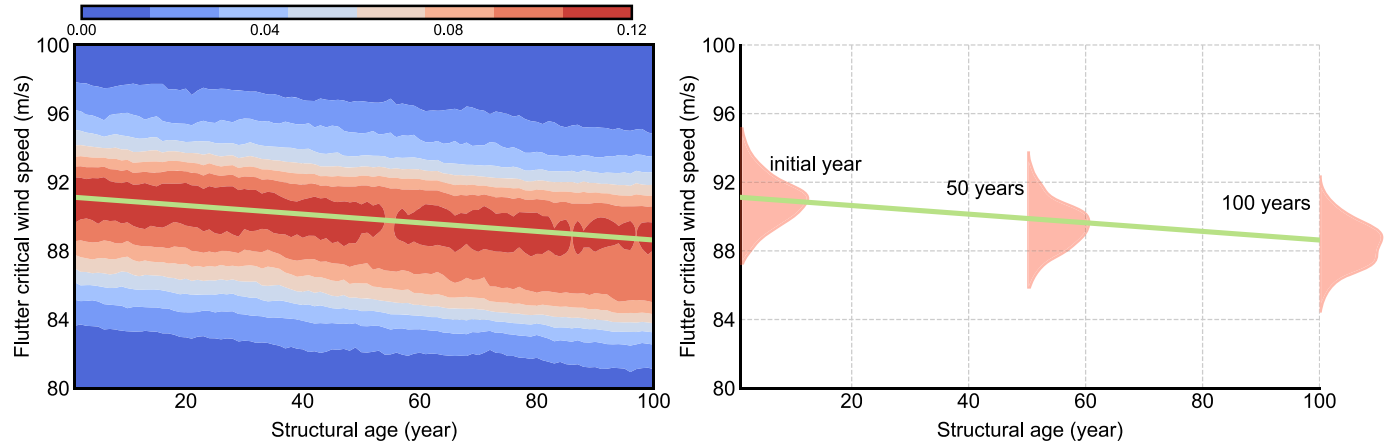

Fig. 13. Life-cycle evolution of flutter critical wind speed's PDF due to deterioration of modal frequencies, considering uncertainty from fitting residuals of modal frequencies, seasonally varying damping ratios, and randomness of FDs.

of the flutter critical wind speed is not as large as that in previous studies (Fang et al. 2020) because in those studies, the uncertainty of FDs was experimental uncertainty, which was much larger than identification uncertainty in this study. It should be stressed that the variations of flutter critical wind speed in each year (caused by the randomness) and in the 100-year period (cased by the structural deterioration, denoted by the green line in Fig. 13) are two different aspects (variation in each year versus variation in the 100-year period). As a result, although the variation caused by the randomness (approximately 8 m/s) was more significant than that caused by the structural deterioration (approximately 2 m/s), the effects of structural deterioration should also be considered.

As mentioned by Chu et al. (2021a) and Cui and Caracoglia (2016), the effects of climate change on annual extreme wind speed are location-dependent. The bridge in this study is located in Zhoushan, China, where the annual extreme wind speed is not sensitive to various climate warming scenarios (Chu et al. 2021a). In order to reveal the potential effects of climate change, we applied the PDF of the annual extreme wind speed for Shenzhen, China, (Fig. 4) on this bridge. Fig. 14 shows the results of life-cycle flutter failure probability under RCP2.6, RCP4.5, and RCP8.5 scenarios. Remarkable discreteness is observed in Fig. 14, which conforms with the conclusions of Chu et al. (2021a) calculated by the generalized density evolution equation. As Fig. 14 shows, the annual flutter failure probability will approximately increase from 0.50×10^{-4} to at most 3.97×10^{-4} under the RCP8.5 scenario.

Time-Variant Probability of Exceeding Predefined Buffeting Response RMS

Fig. 15 shows the life-cycle evolution of buffeting response RMS. The gray planes are the predefined limit of buffeting response RMS, where $\sigma_{\text{lim},h}$ and $\sigma_{\text{lim},\alpha}$ were set as 1.5×10^{-1} and 1.5×10^{-3} for vertical and torsional RMS (Seo and Caracoglia 2012), respectively, for the sake of explanation. The solid lines are the intersecting lines between the RMS surface and the gray planes. The RMS will increase along the reduced velocity, the phenomenon of which was also found by Seo and Caracoglia (2013). With structural aging, the buffeting response RMS will not change generally at various reduced velocities. The torsional RMS at relatively higher reduced velocities will decrease slightly. This decrease may not be caused by the lower estimated accuracy at higher reduced velocities in Fig. 12 because the variation along the structural age axis was mainly due to the structural deterioration [Eq. (4)]. The projected RMS with the structural aging was calculated strictly by Eqs. (4), (7), and (14). As a result, as calculated, the effect of

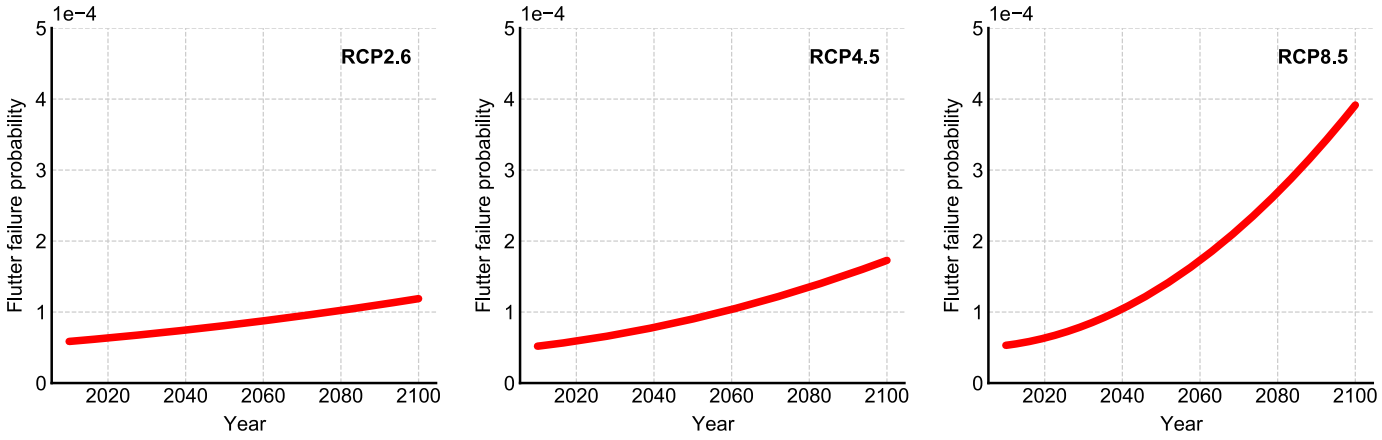

Fig. 14. Life-cycle evolution of flutter failure probability under RCP2.6, RCP4.5, and RCP8.5 climate warming scenarios.

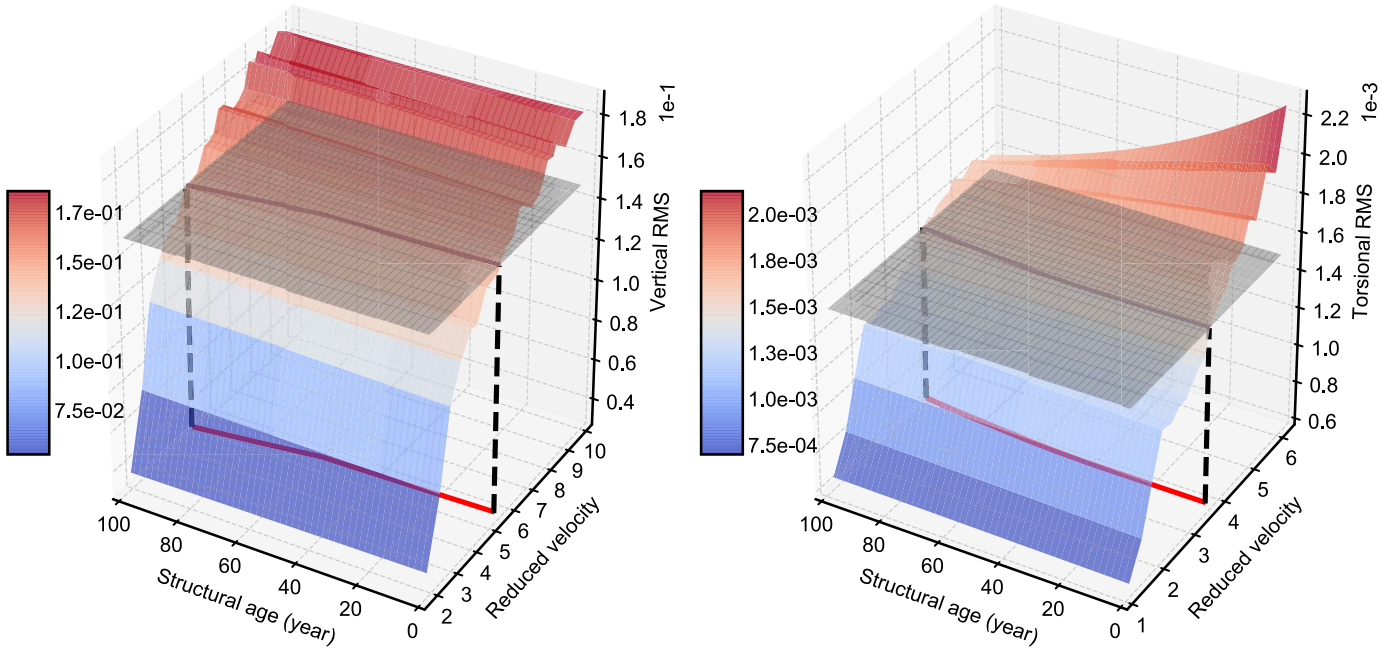

Fig. 15. Life-cycle evolution of buffeting response RMS.

structural deterioration on buffeting RMS was indeed limited. Also, the small waves along the axis of reduced velocity may be caused by numerical approximation, considering the simplification in Eq. (7) and the identification uncertainty in Eq. (9).

The probability of exceeding the predefined RMS limits $\sigma_{\lim,h}$ and $\sigma_{\lim,\alpha}$ is shown in Fig. 16. The variance of exceeding probability was due to the combined action of deteriorating modal frequencies (i.e., structural deterioration) and time-variant Gumbel distribution (i.e., different climate warming scenarios) in Fig. 4. Compared with flutter failure probability, threats from climate change and structural deterioration seem to be of less urgency related to the buffeting response RMS.

Conclusion

This paper proposed a generalized framework for life-cycle assessment of long-span bridges' wind resistant performance, where the time-variant probability of flutter failure and probability of exceeding the predefined limit of buffeting response RMS are the main considered issues. Firstly, this study reviewed the procedure of a full-track TC simulation under three climate warming scenarios based on Vickery's model, where SST served as the representative factor for climate change. The time-variant PDF (due to the warming climate) of extreme wind speed was discussed in detail.

Secondly, the Bayesian system identification approach was introduced. The fast Bayesian FFT method, as an application of Bayesian system identification approach, was utilized to extract a long-span bridge's structural properties (modal frequencies and damping ratios), where the long-term deterioration and seasonally varying phenomena were discussed. The long-term deteriorations are depicted by deteriorating functions. The seasonally varying phenomena are modeled as time-invariant random variables.

Thirdly, a newly proposed Bayesian spectral density approach for identification of flutter derivatives was introduced. The flutter derivatives were extracted in the condition of turbulent flow. The results were compared with those identified in a uniform flow by the traditional least-square method, and satisfactory consistency was found.

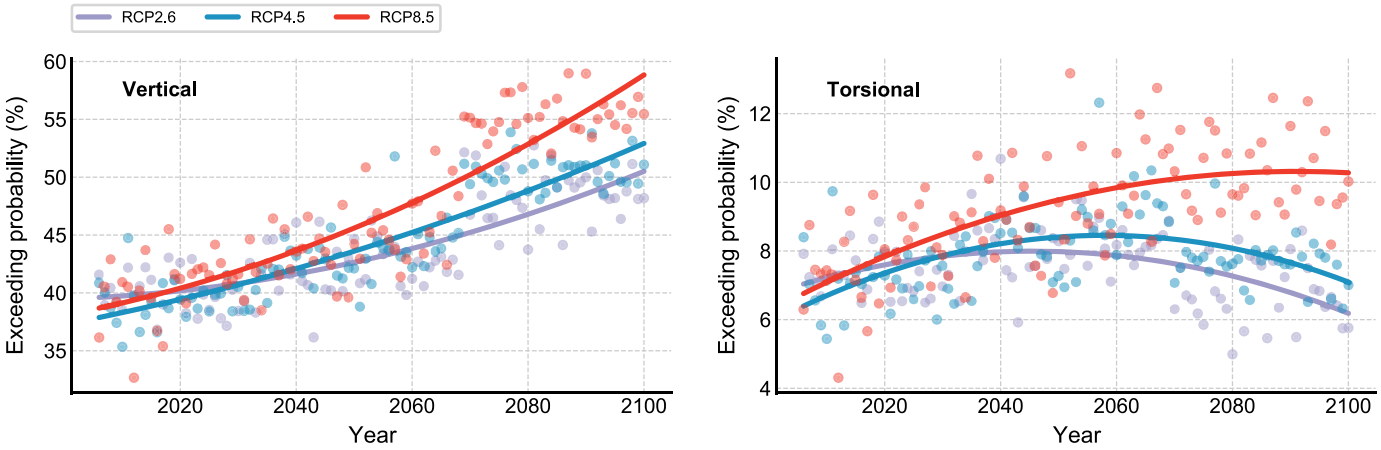

Fig. 16. Life cycle exceeding probability.

The posterior distribution of flutter derivatives, namely identification uncertainty, were quantified by MCMC sampling. Then, the time-variant PDF of flutter critical wind speed was discussed. When estimating the flutter critical wind speed, the time-variant effects included deteriorating parts of modal properties, and the randomness included seasonally varying parts of modal properties and identification uncertainty of flutter derivatives. Hence, the life-cycle flutter failure probability was determined.

Under the RCP8.5 climate warming scenario, the annual flutter failure probability was expected to increase by seven times. In order to reveal the latent deteriorating effects of modal frequencies on buffeting response RMS, the same deteriorating rates of the bridge in this study were employed. The results of flutter derivatives and buffeting force PSDs, identified by Bayesian spectral density approach, were employed and considered as time-invariant in the analysis of buffeting response RMS. Compared with flutter failure probability, the results showed that the combined action of structural deterioration and climate change has a negligible influence on the exceeding probability of buffeting response RMS. As a result, emphasis is suggested to be paid to life-cycle flutter resistant performance.

Data Availability Statement

Some or all data, models, or code that support the findings of this study are available from the corresponding author upon reasonable request.

Acknowledgments

The authors gratefully acknowledge the support of the open funding of the Key Laboratory of Transport Industry of Wind Resistant Technology for Bridge Structures (KLWRTBMC18-01) and National Natural Science Foundation of China (52008314, 51978527, and 52078383). Any opinions, findings, and conclusions are those of the authors and do not necessarily reflect the reviews of the aforementioned agencies.

References

Au, S. 2017. *Operational modal analysis*. New York: Springer.

Au, S.-K. 2011. "Fast Bayesian FFT method for ambient modal identification with separated modes." *J. Eng. Mech.* 137 (3): 214–226. https://doi.org/10.1061/(ASCE)EM.1943-7889.0000213.

Au, S.-K. 2012a. "Fast Bayesian ambient modal identification in the frequency domain, part I: Posterior most probable value." *Mech. Syst. Sig. Process.* 26 (Jan): 60–75. https://doi.org/10.1016/j.ymssp.2011.06.017.

Au, S.-K. 2012b. "Fast Bayesian ambient modal identification in the frequency domain, part II: Posterior uncertainty." *Mech. Syst. Sig. Process.* 26 (Jan): 76–90. https://doi.org/10.1016/j.ymssp.2011.06.019.

Beck, J. L. 2010. "Bayesian system identification based on probability logic." *Struct. Control Health Monit.* 17 (7): 825–847. https://doi.org/10.1002/stc.424.

Brincker, R., L. Zhang, and P. Andersen. 2001. "Modal identification of output-only systems using frequency domain decomposition." *Smart Mater. Struct.* 10 (3): 441. https://doi.org/10.1088/0964-1726/10/3/303.

Caracoglia, L. 2011. "Simulation of linear and non-linear propagation effects of a random turbulence field on bridge flutter instability." *J. Wind Eng. Ind. Aerodyn.* 99 (9): 945–954. https://doi.org/10.1016/j.jweia.2011.06.001.

Chen, X., M. Matsumoto, and A. Kareem. 2000. "Time domain flutter and buffeting response analysis of bridges." *J. Eng. Mech.* 126 (1): 7–16. https://doi.org/10.1061/(ASCE)0733-9399(2000)126:1(7).

Chen, Y., Z. Duan, J. Yang, Y. Deng, T. Wu, and J. Ou. 2021. "Typhoons of western north Pacific basin under warming climate and implications for future wind hazard of East Asia." *J. Wind Eng. Ind. Aerodyn.* 208 (Jan): 104415. https://doi.org/10.1016/j.jweia.2020.104415.

Chu, X., W. Cui, P. Liu, L. Zhao, and Y. Ge. 2022. "Bayesian spectral density approach for identification of bridge section's flutter derivatives operated in turbulent flow." *Mech. Syst. Sig. Process.* 170 (May): 108782. https://doi.org/10.1016/j.ymssp.2021.108782.

Chu, X., W. Cui, L. Zhao, S. Cao, and Y. Ge. 2021a. "Probabilistic flutter analysis of a long-span bridge in typhoon-prone regions considering climate change and structural deterioration." *J. Wind Eng. Ind. Aerodyn.* 215 (Aug): 104701. https://doi.org/10.1016/j.jweia.2021.104701.

Chu, X., H. N. Sinh, W. Cui, L. Zhao, and Y. Ge. 2021b. "Life-cycle assessment for flutter probability of a long-span suspension bridge based on field monitoring data." Preprint, submitted June 20, 2021. http://arxiv.org/abs/2106.10694.

Cui, W., and L. Caracoglia. 2015. "Simulation and analysis of intervention costs due to wind-induced damage on tall buildings." *Eng. Struct.* 87 (Mar): 183–197. https://doi.org/10.1016/j.engstruct.2015.01.001.

Cui, W., and L. Caracoglia. 2016. "Exploring hurricane wind speed along US Atlantic coast in warming climate and effects on predictions of structural damage and intervention costs." *Eng. Struct.* 122 (Sep): 209–225. https://doi.org/10.1016/j.engstruct.2016.05.003.

Cui, W., and L. Caracoglia. 2019. "A new stochastic formulation for synthetic hurricane simulation over the north Atlantic ocean." *Eng. Struct.* 199 (Nov): 109597. https://doi.org/10.1016/j.engstruct.2019.109597.

Cui, W., T. Ma, L. Zhao, and Y. Ge. 2021. "Data-based windstorm type identification algorithm and extreme wind speed prediction." *J. Struct.*

Eng. 147 (5): 04021053. https://doi.org/10.1061/(ASCE)ST.1943-541X.0002954.

Cui, W., L. Zhao, S. Cao, and Y. Ge. 2020. "Bayesian optimization of typhoon full-track simulation on the northwestern Pacific segmented by quadtree decomposition." *J. Wind Eng. Ind. Aerodyn.* 208 (Jan): 104428. https://doi.org/10.1016/j.jweia.2020.104428.

Davenport, A. G. 1961. "A statistical approach to the treatment of wind loading of tall masts and suspension bridges." Ph.D. dissertation, Dept. of Civil Engineering, Univ. of Bristol.

Diana, G., et al. 2020a. "IABSE task group 3.1 benchmark results. Part 1: Numerical analysis of a two-degree-of-freedom bridge deck section based on analytical aerodynamics." *Struct. Eng. Int.* 30 (3): 401–410. https://doi.org/10.1080/10168664.2019.1639480.

Diana, G., et al. 2020b. "IABSE task group 3.1 benchmark results. Part 2: Numerical analysis of a three-degree-of-freedom bridge deck section based on experimental aerodynamics." *Struct. Eng. Int.* 30 (3): 410–420. https://doi.org/10.1080/10168664.2019.1661331.

Ellingwood, B. R., and J. Y. Lee. 2016. "Life cycle performance goals for civil infrastructure: Intergenerational risk-informed decisions." *Struct. Infrastruct. Eng.* 12 (7): 822–829. https://doi.org/10.1080/15732479.2015.1064966.

Fang, G., J. Cao, Y. Yang, L. Zhao, S. Cao, and Y. Ge. 2020. "Experimental uncertainty quantification of flutter derivatives for a PK section girder and its application on probabilistic flutter analysis." *J. Bridge Eng.* 25 (7): 04020034. https://doi.org/10.1061/(ASCE)BE.1943-5592.0001567.

Fang, G., W. Pang, L. Zhao, W. Cui, L. Zhu, S. Cao, and Y. Ge. 2021a. "Extreme typhoon wind speed mapping for coastal region of China: Geographically weighted regression–based circular subregion algorithm." *J. Struct. Eng.* 147 (10): 04021146. https://doi.org/10.1061/(ASCE)ST.1943-541X.0003122.

Fang, G., W. Pang, L. Zhao, P. Rawal, S. Cao, and Y. Ge. 2021b. "Toward a refined estimation of typhoon wind hazards: Parametric modeling and upstream terrain effects." *J. Wind Eng. Ind. Aerodyn.* 209 (Feb): 104460. https://doi.org/10.1016/j.jweia.2020.104460.

Fang, G., L. Zhao, L. Song, X. Liang, L. Zhu, S. Cao, and Y. Ge. 2018. "Reconstruction of radial parametric pressure field near ground surface of landing typhoons in northwest Pacific Ocean." *J. Wind Eng. Ind. Aerodyn.* 183 (Dec): 223–234. https://doi.org/10.1016/j.jweia.2018.10.020.

Flato, G., G. Boer, W. Lee, N. McFarlane, D. Ramsden, M. Reader, and A. Weaver. 2000. "The Canadian Centre for climate modelling and analysis global coupled model and its climate." *Clim. Dyn.* 16 (6): 451–467. https://doi.org/10.1007/s003820050339.

Georgiou, P. N. 1986. *Design wind speeds in tropical cyclone-prone regions*. London, ON, Canada: Faculty of Graduate Studies, Univ. of Western Ontario.

Gu, M., and X.-R. Qin. 2004. "Direct identification of flutter derivatives and aerodynamic admittances of bridge decks." *Eng. Struct.* 26 (14): 2161–2172. https://doi.org/10.1016/j.engstruct.2004.07.015.

Gu, M., Y. L. Xu, L. Chen, and H. Xiang. 1999. "Fatigue life estimation of steel girder of yangpu cable-stayed bridge due to buffeting." *J. Wind Eng. Ind. Aerodyn.* 80 (3): 383–400. https://doi.org/10.1016/S0167-6105(98)00209-8.

Hermans, L., and H. Van der Auweraer. 1999. "Modal testing and analysis of structures under operational conditions: Industrial applications." *Mech. Syst. Sig. Process.* 13 (2): 193–216. https://doi.org/10.1006/mssp.1998.1211.

Hong, X., A. Kareem, and J. Li. 2020. "Validation of the fast intensity model for typhoon and its application to the estimation of typhoon wind hazard for the southeast coast of China." *J. Wind Eng. Ind. Aerodyn.* 206 (Nov): 104379. https://doi.org/10.1016/j.jweia.2020.104379.

Hong, X., and J. Li. 2021. "A beta-advection typhoon track model and its application for typhoon hazard assessment." *J. Wind Eng. Ind. Aerodyn.* 208 (Jan): 104439. https://doi.org/10.1016/j.jweia.2020.104439.

Hwang, Y. C., S. Kim, and H.-K. Kim. 2020. "Cause investigation of high-mode vortex-induced vibration in a long-span suspension bridge." *Struct. Infrastruct. Eng.* 16 (1): 84–93. https://doi.org/10.1080/15732479.2019.1604771.

Ibrahim, S. 1977. "Random decrement technique for modal identification of structures." *J. Spacecraft Rockets* 14 (11): 696–700. https://doi.org/10.2514/3.57251.

James, G. H., III, T. G. Carne, and J. P. Lauffer. 1993. *The natural excitation technique (next) for modal parameter extraction from operating wind turbines*. Albuquerque, NM: Sandia National Labs.

Ji, X., G. Huang, and Y.-G. Zhao. 2020. "Probabilistic flutter analysis of bridge considering aerodynamic and structural parameter uncertainties." *J. Wind Eng. Ind. Aerodyn.* 201 (Jun): 104168. https://doi.org/10.1016/j.jweia.2020.104168.

Ji, X., Y.-G. Zhao, and Z.-H. Lu. 2021. "Uncertainty analysis of bridge flutter considering dependence and sampling error in flutter derivative measurements." *Eng. Struct.* 246 (Nov): 113051. https://doi.org/10.1016/j.engstruct.2021.113051.

Katafygiotis, L. S., and K.-V. Yuen. 2001. "Bayesian spectral density approach for modal updating using ambient data." *Earthquake Eng. Struct. Dyn.* 30 (8): 1103–1123. https://doi.org/10.1002/eqe.53.

Knapp, K. R., H. J. Diamond, J. P. Kossin, M. C. Kruk, and C. J. Schreck. 2018. "International best track archive for climate stewardship (IBTrACS) project, version 4." Accessed November 12, 2020. https://data.nodc.noaa.gov/cgi-bin/iso?id=gov.noaa.ncdc:C01552.

Krishnaiah, P. 1976. "Some recent developments on complex multivariate distributions." *J. Multivariate Anal.* 6 (1): 1–30. https://doi.org/10.1016/0047-259X(76)90017-8.

Lee, J. Y., and B. R. Ellingwood. 2017. "A decision model for intergenerational life-cycle risk assessment of civil infrastructure exposed to hurricanes under climate change." *Reliab. Eng. Syst. Saf.* 159 (Mar): 100–107. https://doi.org/10.1016/j.ress.2016.10.022.

Li, H., S. Laima, J. Ou, X. Zhao, W. Zhou, Y. Yu, N. Li, and Z. Liu. 2011. "Investigation of vortex-induced vibration of a suspension bridge with two separated steel box girders based on field measurements." *Eng. Struct.* 33 (6): 1894–1907. https://doi.org/10.1016/j.engstruct.2011.02.017.

Li, J., and J. Chen. 2009. *Stochastic dynamics of structures*. London: Wiley.

Li, J., and X. Hong. 2021. "Typhoon hazard analysis based on the probability density evolution theory." *J. Wind Eng. Ind. Aerodyn.* 219 (Dec): 104796. https://doi.org/10.1016/j.jweia.2021.104796.

Liu, P., L. Zhao, G. Fang, and Y. Ge. 2021. "Explicit polynomial regression models of wind characteristics and structural effects on a long-span bridge utilizing onsite monitoring data." *Struct. Control Health Monit.* 28 (5): e2705. https://doi.org/10.1002/stc.2705.

Mannini, C., and G. Bartoli. 2015. "Aerodynamic uncertainty propagation in bridge flutter analysis." *Struct. Saf.* 52 (Jan): 29–39. https://doi.org/10.1016/j.strusafe.2014.07.005.

Melchers, R. E., and A. T. Beck. 2018. *Structural reliability analysis and prediction*. Chichester, UK: Wiley.

Nguyen, A., K. T. L. Kodikara, T. H. Chan, and D. P. Thambiratnam. 2019. "Deterioration assessment of buildings using an improved hybrid model updating approach and long-term health monitoring data." *Struct. Health Monit.* 18 (1): 5–19. https://doi.org/10.1177/1475921718799984.

Pant, S., and E. J. Cha. 2019. "Potential changes in hurricane risk profile across the United States coastal regions under climate change scenarios." *Struct. Saf.* 80 (Sep): 56–65. https://doi.org/10.1016/j.strusafe.2019.05.003.

Peng, Z., W. T. Peter, and F. Chu. 2005. "An improved Hilbert–Huang transform and its application in vibration signal analysis." *J. Sound Vib.* 286 (1–2): 187–205. https://doi.org/10.1016/j.jsv.2004.10.005.

Salawu, O. 1997. "Detection of structural damage through changes in frequency: A review." *Eng. Struct.* 19 (9): 718–723. https://doi.org/10.1016/S0141-0296(96)00149-6.

Sarkar, P. P., N. P. Jones, and R. H. Scanlan. 1992. "System identification for estimation of flutter derivatives." *J. Wind Eng. Ind. Aerodyn.* 42 (1–3): 1243–1254. https://doi.org/10.1016/0167-6105(92)90131-S.

Scanlan, R. H. 1993. "Problematics in formulation of wind-force models for bridge decks." *J. Eng. Mech.* 119 (7): 1353–1375. https://doi.org/10.1061/(ASCE)0733-9399(1993)119:7(1353).

Scanlan, R. H., and J. Tomo. 1971. "Air foil and bridge deck flutter derivatives." *J. Soil Mech. Found. Div.* 97 (6): 1717–1737. https://doi.org/10.1061/JMCEA3.0001526.

Seo, D.-W., and L. Caracoglia. 2011. "Estimation of torsional-flutter probability in flexible bridges considering randomness in flutter derivatives." *Eng. Struct.* 33 (8): 2284–2296. https://doi.org/10.1016/j.engstruct.2011.03.016.

Seo, D.-W., and L. Caracoglia. 2012. "Statistical buffeting response of flexible bridges influenced by errors in aeroelastic loading estimation." *J. Wind Eng. Ind. Aerodyn.* 104 (May): 129–140. https://doi.org/10.1016/j.jweia.2012.03.036.

Seo, D.-W., and L. Caracoglia. 2013. "Estimating life-cycle monetary losses due to wind hazards: Fragility analysis of long-span bridges." *Eng. Struct.* 56 (Nov): 1593–1606. https://doi.org/10.1016/j.engstruct.2013.07.031.

Seo, D.-W., and L. Caracoglia. 2015. "Exploring the impact of 'climate change' on lifetime replacement costs for long-span bridges prone to torsional flutter." *J. Wind Eng. Ind. Aerodyn.* 140 (May): 1–9. https://doi.org/10.1016/j.jweia.2015.01.013.

Shen, Z., and K. Wei. 2021. "Stochastic model of tropical cyclones along China coast including the effects of spatial heterogeneity and ocean feedback." *Reliab. Eng. Syst. Saf.* 216 (Dec): 108000. https://doi.org/10.1016/j.ress.2021.108000.

Siedziako, B., O. Øiseth, and A. Rønnquist. 2017. "An enhanced forced vibration rig for wind tunnel testing of bridge deck section models in arbitrary motion." *J. Wind Eng. Ind. Aerodyn.* 164 (May): 152–163. https://doi.org/10.1016/j.jweia.2017.02.011.

Snaiki, R., and T. Wu. 2020. "Revisiting hurricane track model for wind risk assessment." *Struct. Saf.* 87 (Nov): 102003. https://doi.org/10.1016/j.strusafe.2020.102003.

Snaiki, R., T. Wu, A. S. Whittaker, and J. F. Atkinson. 2020. "Hurricane wind and storm surge effects on coastal bridges under a changing climate." *Transp. Res. Rec.* 2674 (6): 23–32. https://doi.org/10.1177/0361198120917671.

Spence, S. M., and A. Kareem. 2014. "Performance-based design and optimization of uncertain wind-excited dynamic building systems." *Eng. Struct.* 78 (Nov): 133–144. https://doi.org/10.1016/j.engstruct.2014.07.026.

Stocker, T. 2014. *Climate change 2013: The physical science basis: Working group I contribution to the fifth assessment report of the Intergovernmental Panel on Climate Change*. New York: Cambridge Univ. Press.

Van Vuuren, D. P., et al. 2011. "The representative concentration pathways: An overview." *Clim. Change* 109 (1–2): 5. https://doi.org/10.1007/s10584-011-0148-z.

Vickery, P., P. Skerlj, and L. Twisdale. 2000a. "Simulation of hurricane risk in the US using empirical track model." *J. Struct. Eng.* 126 (10): 1222–1237. https://doi.org/10.1061/(ASCE)0733-9445(2000)126:10(1222).

Vickery, P. J., P. Skerlj, A. Steckley, and L. Twisdale. 2000b. "Hurricane wind field model for use in hurricane simulations." *J. Struct. Eng.* 126 (10): 1203–1221. https://doi.org/10.1061/(ASCE)0733-9445(2000)126:10(1203).

Wang, Y., C. Zhang, Y. Ni, and X. Xu. 2022. "Bayesian probabilistic assessment of occupant comfort of high-rise structures based on structural health monitoring data." *Mech. Syst. Sig. Process.* 163 (Jan): 108147. https://doi.org/10.1016/j.ymssp.2021.108147.

Wu, F., G. Huang, and X. Zhou. 2021a. "Enhanced circular subregion method in typhoon hazard analysis." *J. Struct. Eng.* 147 (6): 06021003. https://doi.org/10.1061/(ASCE)ST.1943-541X.0003003.

Wu, Y., X. Chen, and Y. Wang. 2021b. "Identification of linear and nonlinear flutter derivatives of bridge decks by unscented Kalman filter approach from free vibration or stochastic buffeting response." *J. Wind Eng. Ind. Aerodyn.* 214 (Jul): 104650. https://doi.org/10.1016/j.jweia.2021.104650.

Xia, Y., H. Hao, G. Zanardo, and A. Deeks. 2006. "Long term vibration monitoring of an RC slab: Temperature and humidity effect." *Eng. Struct.* 28 (3): 441–452. https://doi.org/10.1016/j.engstruct.2005.09.001.

Xu, H., N. Lin, M. Huang, and W. Lou. 2020. "Design tropical cyclone wind speed when considering climate change." *J. Struct. Eng.* 146 (5): 04020063. https://doi.org/10.1061/(ASCE)ST.1943-541X.0002585.

Xu, Y. L., T. Liu, and W. Zhang. 2009. "Buffeting-induced fatigue damage assessment of a long suspension bridge." *Int. J. Fatigue* 31 (3): 575–586. https://doi.org/10.1016/j.ijfatigue.2008.03.031.

Yuen, K.-V. 2010. *Bayesian methods for structural dynamics and civil engineering*. Singapore: Wiley.

Yuen, K.-V., and L. S. Katafygiotis. 2001. "Bayesian time–domain approach for modal updating using ambient data." *Probab. Eng. Mech.* 16 (3): 219–231. https://doi.org/10.1016/S0266-8920(01)00004-2.

Yuen, K.-V., and L. S. Katafygiotis. 2003. "Bayesian fast fourier transform approach for modal updating using ambient data." *Adv. Struct. Eng.* 6 (2): 81–95. https://doi.org/10.1260/136943303769013183.

Yuen, K.-V., and S.-C. Kuok. 2010. "Ambient interference in long-term monitoring of buildings." *Eng. Struct.* 32 (8): 2379–2386. https://doi.org/10.1016/j.engstruct.2010.04.012.

Zhang, J., L. Zhou, Y. Tian, S. Yu, W. Zhao, and Y. Cheng. 2021. "Vortex-induced vibration measurement of a long-span suspension bridge through noncontact sensing strategies." *Comput.-Aided Civ. Infrastruct. Eng.* https://doi.org/10.1111/mice.12712.

Zhao, L., W. Cui, and Y. Ge. 2019. "Measurement, modeling and simulation of wind turbulence in typhoon outer region." *J. Wind Eng. Ind. Aerodyn.* 195 (Dec): 104021. https://doi.org/10.1016/j.jweia.2019.104021.

Zhao, L., X. Xie, Y.-Y. Zhan, W. Cui, Y.-J. Ge, Z.-C. Xia, S.-Q. Xu, and M. Zeng. 2020. "A novel forced motion apparatus with potential applications in structural engineering." *J. Zhejiang Univ.-Sci. A* 21 (7): 593–608. https://doi.org/10.1631/jzus.A1900400.